University of South-Eastern Norway

www.usn.no

FMH606 Master's Thesis 2020

Process Technology

Assessment of CFD methods in predicting flow pattern and pressure gradient in two phase gas-liquid vertical flow

Navid Pouladi

Faculty of Technology, Natural sciences and Maritime Sciences

Campus Porsgrunn

University of South-Eastern Norway

www.usn.no

Course: FMH606 Master's Thesis, 2020

Title: Assessment of CFD methods in predicting flow regime and pressure gradient in two phase gas-liquid vertical flow

Number of pages: 58

Keywords: CFD, two-phase, gas-liquid, vertical upward flow, flow pattern, multifluid Eulerian, VOF, interfacial area concentration

Student: Navid Pouladi

Supervisor: Britt Margrethe Emilie Moldestad

External partner: Haavard Aakre

Availability: Open

Summary:

Available tools for dealing with multi-phase flows are not effective with complex geometries such as process piping with combination of horizontal and vertical pipes, bends and valves. However, rapid development of computation power has made CFD a more applicable tool in this field. This study aims to suggest and assess a CFD method to deal with all flow patterns existing in a vertical two-phase gas-liquid upward flow.

A multi-fluid approach has been suggested where the Multifluid Eulerian and Volume of Fluid (VOF) methods are used together, in combination with the interfacial area concentration (IAC) equation.

The CFD results regarding flow pattern, void fraction and pressure gradient have been compared to experimental results and a relatively good agreement has been observed. The study found that the IAC equation plays an important role in predicting flow patterns. However, a more sophisticated IAC equation and better models for bubble coalescence and break-up could lead to a better performance of the multifluid model suggested.

The study concludes that the CFD method suggested is a reliable and applicable tool for more complex geometries. However, further work is required to ensure this.

Preface

In searching for a CFD method which can be used for various flow patterns of gas-liquid flows, the author found just one publication dealing with this issue. The majority of works dedicated to CFD modeling of two-phase flows are focused on a specific flow pattern and have developed a model which could just be used for that specific flow pattern. This is the bottleneck for using CFD for engineering applications of multiphase flows. Specially where the flow pattern is not known from the beforehand or a fully developed flow pattern does not exist because of complex geometry, etc.

This work has tried to break this bottleneck and suggest a model which is capable of handling various flow patterns in gas-liquid flows. In order to be able to verify this model, a vertical upward flow, where the flow patterns are relatively defined for it, has been chosen as the case study.

This study starts by reviewing major works done before in this field and continues with introducing available CFD models for multiphase flows. The task and the suggested CFD model for dealing with it, has been presented in chapter four. Finally, the results have been presented and analyzed in relation to the CFD model used.

Arendal, 14.05.2020

Navid Pouladi

Contents

Nomenclature

A	Area	m^2
A_p	Interfacial area concentration	$\frac{1}{m}$
C_D	Drag coefficient	
C_l	Lift Coefficient	
C_{TD}	Turbulence dispersion coefficient	
C_{vm}	Virtual mass coefficient	
C_{wl}	Wall lubrication coefficient	
D	Diameter of pipe	m
d	Bubble/droplet diameter	m
F	External force	N
f	Friction factor	
G	Generation of turbulence kinetic energy	$\frac{kg}{m.s^3}$
g	Gravitational acceleration	$\frac{m}{s^2}$
HL	Liquid holdup	
K	Interphase momentum exchange coefficient	
k	Kinetic energy	$\frac{m^2}{s^2}$
$\dot{m}$	Mass transfer rate	$\frac{kg}{s}$
n	Number of phases	
R	Interphase force	N
Re	Reynolds number	
S	Source term	
v	Velocity	$\frac{m}{s}$

Greek Letters

α	Void fraction	
ε	Dissipation rate of kinetic energy	$\frac{m^2}{s^3}$
μ	Dynamic viscosity	$Pa.s$
ω	Turbulence frequency	$\frac{1}{s}$
ρ	Density	$\frac{kg}{m^3}$
τ	Shear stress	Pa

Superscripts

T	Transpose of matrix

Subscripts

g	Gas
l	Liquid
m	Mixture
p	Secondary phase
q	Primary phase
dr	Drift

Abbreviations

CFD	Computational Fluid Dynamics
CFL	Courant–Friedrichs–Lewy number
DNS	Direct Numerical Simulation
ECT	Electrical Capacitance Tomography
EIT	Electrical Impedance Tomography
IAC	Interfacial Area Concentration

LES	Large Eddy Simulation
LHS	Left Hand Side
PBE	Population Balance Equation
PDF	Probability Density Function
PSD	Particle Size Distribution
QMOM	Quadrature Method of Moments
RANS	Reynolds Averaged Navier-Stokes
RSM	Reynolds Stress Model
RHS	Right Hand Side
UDF	User-Defined Functions
URF	Under-Relaxation Factor
VOF	Volume Of Fluid
WMS	Wire Mesh Sensor

1 Introduction

From the nature we live in, to multiple applications in the industry, multiphase flows occur everywhere. These flows could be various combinations of liquid-gas, liquid-liquid, liquid- gas-solid, liquid-solid, etc. Dealing with each one of these combinations of phases has its own complications and researchers and engineers have developed many different methods to deal with multiphase flows.

Despite the broad work has been done during the years in dealing with multiphase flows, the complex nature of these flows make it a difficult task to develop models which can simulate the behavior of these flows. Hence, multiphase flows are still fairly an open area of research. Computational fluid dynamics, CFD, is progressively being used for modeling of multiphase flows. This work is an effort to investigate the applicability and efficiency of using CFD for a specific multiphase flow category.

1.1 Motivation and background

Flow assurance deals with safe, economic and optimized flow of fluids in the flow path. Multiphase flows are quite common in the oil industry. The very normal production flows from an oil reservoir are a combination of liquid and gas hydrocarbons, water and sand. There are variety of tools which have been developed during the years to take care of flow assurance problems. Empirical correlations, mechanistic models and commercial software, to ease the task of flow assurance for multiphase flows.

These methods and tools are developed for one, two or three dimensional, steady-state or transient flow, and could be simple or more sophisticated; but they are generally developed for a common flow path, circular pipe or riser. It may be possible to include piping and valve details, to some degree, in some of these tools, but generally these tools and models cannot handle complexity of the geometry. As part of my job working with the flow assurance, I have encountered process systems with combination of pipes, pipe bends, valves, reducers and expanders, manifolds, swivels etc. The task of flow assurance for such combination could be challenging enough for one-phase flow and the results are often an approximate. For the multiphase flow however, this is quite challenging. As the result of this complexity, the systems designed for multiphase flows are commonly based on a conservative approximation which is unnecessarily expensive.

CFD software are not common in large piping and valve systems. The reason is the that CFD demands enormous computing power for a large, three-dimensional arrangement. However, the computing power is advancing with a rapid pace. Cloud-based computing, where supercomputers can be used remotely, is getting more and more common and popular. Therefore, using CFD for small and medium sized process systems is a possibility now, and the cost of simulating and computing could be modest comparing to a possible saving a company could make designing an optimized system and avoiding an oversized process system. This is especially applicable to a multiphase process system where there is no comparable good options.

CFD methods for multiphase flows could be relatively complex. In general, a good understanding of both the nature of the flow and the equations and computational methods being used is needed. This is another challenge in using CFD for multiphase flow process engineering applications. Besides, verification of CFD results is not straightforward and it is easy to get misleading and erroneous results. A specific model is needed, not only for each type of multiphase flow, but also for the specific flow characteristics and pattern under study.

CFD is not a young science, but because of the limitations mentioned above the engineering use of CFD for multiphase process flows is underdeveloped. Consequently, the experience and literature around this is also relatively limited. With the significant advances in the computation capacity and the growing access to the cloud-based computing, it is expected that CFD will become a more common tool for engineering applications of multiphase flows in process systems.

1.2 Objective

A common type of multiphase flow encountered in the process industry is the two-phase gas-liquid flow. A general discussion regarding the CFD methods for multiphase gas-liquid flows is a comprehensive project. This work has chosen a special case: air-water two-phase vertical upward flow in a pipe. The reason for choosing this case is that there is enough experimental results for this case, to be able to verify the CFD results with the experimental results. There are also some good works in the literature, which have used CFD for modeling of vertical upward gas-liquid flows. However, most of these works have discussed a specified flow pattern. For the objective of this work, which is to assess the use of CFD as an engineering tool in process systems, this is not favorable. For the type of process piping, valves and components mentioned earlier, the defined fully developed flow patterns do not exist.

This work aims to assess the performance of CFD for the special case of gas-liquid flow chosen, in prediction of the flow pattern and other characteristics such as void fraction and pressure drop. This study hope to be able to conclude that for the special case studied here, a single CFD method can predict flow pattern and other characteristics with an acceptable accuracy for engineering applications. Then it may be possible to conclude that this model can further be used for more complex geometries, where the defined flow patterns do not exist.

1.3 Definitions

Some of the basic definitions used in this study without prior explanation are listed below:

- Superficial velocity: The velocity obtained, if the entire cross section of the flow path was filled with just one of the phases. It is defined as the flow rate of gas or liquid divided by the cross-section area of the pipe:
  $v_{sl} = \frac{Q_l}{A}$ and $v_{sg} = \frac{Q_g}{A}$
- Slip velocity: Also called drift velocity, is the difference between velocity of the phases. For example, the difference between the velocity of liquid and a rising bubble
  $v_{dr} = v_g - v_l$
- Void fraction: The ratio of volume occupied by the gas phase to the total volume of the flow domain
- Liquid holdup: The ratio of the volume occupied by liquid to the total volume of the flow domain. It is connected to void fraction as:
  $HL = 1 - \propto$
- Small/large pipe: Large pipes are designated from small pipes based on the finding that a large rising gas bubble, known as Taylor bubble, cannot occupy the whole cross section of the pipe. In this manner, Kataoka & Ishii [1] defined a large pipe as a pipe diameter larger than:

$$D = 40\sqrt{\frac{\sigma}{g(\rho_l - \rho_g)}} \qquad 1\text{-}1$$

For air-water two-phase flow at normal operating conditions this corresponds to a diameter of 108mm.

- Constitutive models: Also called closure models are equations needed in addition to conservation laws in order to have enough equations for all the variables for interphase interactions and other phenomena not captured by the main model equations

1.4 Overview of the thesis structure

Chapter 2 starts with a short introduction of general approaches to gas-liquid two-phase flows. A structured literature review regarding CFD approaches specifically used for vertical upward gas-liquid flows has been presented. Further, two phase flow patterns and flow pattern maps developed by researchers in the past has been discussed.
Chapter 3 discusses the theoretical background for CFD modelling of gas-liquid flows. The main equations and models are presented and discussed.
Chapter 4 primarily defines the case study chosen for this thesis. The experimental reference used for verifying the CFD results has been introduced. A CFD model has been suggested based on the theory represented in Chapter 3.
Chapter 5 represents the results for the case study and compares them with the experimental reference. Discussions regarding the efficiency of the suggested model and the possibility for generalization of it are given here.
Chapter 6 represents the main conclusions obtained from the study of CFD models for gas-liquid flows.

2 Background and literature review

The aim of this chapter is to construct the basis to introduce the problem and further the approach to solve the problem. The literature review part goes through similar tasks done in the past publications. A background for general approaches to two-phase flow problems is introduced. Issues regarding flow patterns in two phase vertical upward flow and flow pattern maps are discussed in this chapter.

2.1 Approaches to two-phase flow problem

2.1.1 Mechanistic models

There are plenty of mechanistic models in the literature and it is not straightforward to categorize them. However, it is possible to put these mechanistic models in three main categories:

- Mixture models
- Drift flux models
- Multifluid models

The **mixture models**, in some publications called homogeneous model, assumes that the velocity of phases, as well as pressure and temperature are equal. The mixture model commonly solves a continuity equation for each phase, but the momentum and energy equations are solved for the mixture. The fluid properties are average properties of the mixture. This model could not be used when the slip velocity between two phases is not negligible

The **Drift flux models**, are a modification of the mixture model, based on the assumption of local equilibrium over short spatial length scales. It also uses one momentum equation for the mixture. Though, an extra algebraic equation is used to take care of velocity differences between the phases. There are a broad range of drift flux models in the literature with different slip velocity correlations and closure models.

The **multifluid models**, solve a separate set of conservation equations for each phase involved. They are commonly called two fluid model or three fluid model based on the number of separate equations used for dealing with the multi-phase phenomenon. For gas-liquid flows, A two fluid model solves separate conservation equations for the gas and fluid phases. However, a third set of equations may be used for dealing with droplets or bubbles. The phase equations may be coupled, in a way that the pressure is assumed equal for all phases; or segregated. When the compressibility of the gas phase is also important, it results in a more complicated model.

2.1.2 Empirical correlations

Empirical and semi-empirical correlations have a long history in all applications dealing with multiphase flows. Engineers have specially used correlations more frequently than other methods due to the convenient and easy use of them. However, most of these correlations are aimed for a defined area of application. Even in the defined area of applications correlations are not completely reliable and deviations for the obtained results could be quite high.

The majority of correlations available in the literature are developed for a specific flow regime. Some correlations are more general but they use somehow a flow regime identification as well. A major problem with correlations is that most of them are developed based on the data sets for small pipes and therefore the uncertainty level is higher when using them for larger diameter pipes [2]. Most of the correlations are originally developed for horizontal flow and modified for pipe inclinations afterwards. Woldesemayat & Ghajar [3], analyzed the performance of 68 void fraction correlations and developed a general correlation, which could predict void fraction efficiently for the range of datasets, in the different flow regimes they investigated. Beggs & Brill correlation is used extensively in the oil industry. According to Behnia [2], this correlation is closest approximation for pressure gradient. This correlation has been used and introduced in Chapter 5.

2.1.3 Commercial software

OLGA, owned by Schlumberger, was originally developed by SINTEF and Institute for Energy Technology (IFE). OLGA is an extended two-fluid model (actually a three-fluid model) which solves conservation equations for the gas and liquid phase as well as droplets [4]. OLGA has been extensively used in petroleum industry since the 80s.

LedaFlow, owned by Kongsberg Oil & Gas Technologies, was also developed by SINTEF; and sponsored by TOTAL and ConocoPhillip. The parameters used in the mechanistic model developed, were adjusted based on the SINTEF 8″ and 12″ loop in Tiller. The author could not find a publication showing the principle of work of this code.

There has been several assessment programs for comparing OLGA and LedaFlow for different transient multiphase scenarios [5]. Both codes are found to give relatively similar results.

TACITE was developed by French Petroleum Institute (IFP) and TotalFinaElf. It uses a drift flux model with separate continuity equations for the gas and liquid phase, but a mixture model for momentum and energy conservation [6].

There are some other commercial codes available in the market. It should be noted that these software are designed for pipelines and pipe networks. Hence, they cannot be used for complex geometries.

2.2 Literature review

A comprehensive literature review regarding all the approaches to two-phase vertical upward flow may be useful, but the diversity of methods make it difficult to come to a conclusion, which could further be used for the aim of this work. Dealing generally with computational methods used for two-phase gas-liquid vertical upward flow also involves many publications, which have introduced a mechanistic model and have solved the equations by discretizing them in time and space domain. A goal-oriented way has been chosen here to introduce publications which have used CFD tools with the recognized approaches for CFD modeling of multiphase flows as discussed in Chapter 3. summarizes the major aspects of these publications:

Table 2 1: Summary of the literature review

Publication	Year	Software	Method	Pipe Size(s)	Flow Pattern(s)	Turbulence model	fluids
Liu et al. [7]	2011	ANSYS FLUENT 6.3.26	VOF	31.8mm	Annular	Low Reynolds *k-ε*	Air-water
Dakshinammorthy et al. [8]	2013	ANSYS FLUENT 14.5	Eulerian–Eulerian multifluid VOF	189mm	Bubble, intermittent, semi annular, annular	*k-ω*	Air-water
Abdulkadir et al. [9]	2015	Star-CCM+	VOF	67mm	Slug	*k-ε*	air–silicone oil
Parsi et al. [10]	2016	ANSYS FLUENT 15	Eulerian–Eulerian multifluid VOF	76mm	Churn	RNG k-ε & SST *k-ω*	Air-water
Peña-Monferrer et al. [11]	2016	OpenFOAM	Eulerian–Eulerian and population balance	52mm	Bubble	*k-ε*	Air-water
Tocci et al. [12]	2017	OpenFOAM	Eulerian–Eulerian multifluid VOF	50.8mm, 67mm	Churn and Slug	SST *k-ω*	Air-water
Zahedi et al. [13]	2017	ANSYS FLUENT 14.5	VOF & Eulerian–Eulerian multifluid VOF	76.2mm	Annular	RSM/ SST *k-ω*	Air-water
Abood et al. [14]	2019	ANSYS FLUENT 16.1	VOF	24mm	Bubble, cap bubble, slug, churn, annular	RNG *k-ε*	Air-oil
Adaze et al. [15]	2019	ANSYS FLUENT 16.1	Eulerian–Eulerian multifluid VOF	76.2mm	Annular	*k-ε*	Air-water

Liu et al. [7] used the VOF model to simulate air-water annular flow in a 31.8mm vertical pipe. They used a two-dimensional geometry with axis as the symmetry boundary condition. The authors used a creative method and programmed source terms in the mass, momentum, turbulence kinetic energy and turbulence dissipation rate equations by UDFs (user defined functions). The authors then defined these source terms by suitable correlations for the annular flow from the literature. The source term in the continuity equation accounts for the entrainment and deposition of droplets between the gas core to the wall film. The momentum transfer between the gas core and film is captured through the source term in the momentum equation. The source terms in the turbulence kinetic energy and turbulence dissipation rates then capture the inter-phase turbulence transfer. Finally, the source term in the VOF equation captures the interfacial entrainment and deposition processes. This work has then compared results for entrainment fraction, pressure gradient and film thickness with the experimental results and correlations; which are in a relatively good agreement.

Dakshinammorthy et al. [8] from the ANSYS Inc. published one of the rare works claiming that a general CFD model can be used to simulate all flow regimes without prior knowledge of the flow regime, instead of an adapted CFD model for each specific flow regime. The authors used Eulerian-Eulerian multifluid VOF approach to compare with experimental results for a riser with 189 mm internal diameter. They simulated four cases of bubble, intermittent, semi annular and annular flow of naphtha and nitrogen. They took liquid as the primary, continuous, phase and the secondary phase, gas, is then forming the bubbles. The study uses k-ω turbulence model with turbulence damping. The closure equations are an anisotropic drag and Tomiyama [16] model has been used for the lift force, available in ANSYS Fluent. The wall lubrication force has also been modeled by Tomiyama [16] model. The authors used interfacial area concentration transport equation, which includes source terms to account for coalescence and break-up of bubbles. The correlation used via these source terms are Hibiki & Ishii [17] for binary break-up of bubbles and Wu et al. [18] for bubble coalescence. The work provides contours of void fraction for the pipe axial and lateral section to show how the model captures expected flow regime. Finally, the pressure gradient and void fraction results has been compared with the experiment. The results are fairly satisfactory, the deviation for the pressure gradient is a little bit higher for some cases.

Abdulkadir et al. [9] studied slug flow of air and silicone oil mixture in a 67mm acrylic pipe of 6m length. The authors used an experimental setup with ECT (Electrical Capacitance Tomography) and WMS (Wire Mesh Sensor). The VOF method has been used to compare CFD results with the experiment. Authors used a three-dimensional butterfly mesh and performed a mesh sensitivity analysis for six meshes from coarser to finer. Void fraction and PDF (Probability Density Function) are compared for the CFD results and sensors read at the same elevation of the pipe. The study shows that the CFD method used can simulate the flow pattern and the special characteristics of slug flow: the formation of Tylor bubbles, the falling liquid film and the entrained bubbles in the wake of the Tylor bubble. The length of the Tylor bubble could be simulated correctly but there was a 20% error in slug frequency prediction. The results were also satisfactory for the void fraction and the pressure gradient.

Parsi et al. [10] studied churn flow of air-water mixture in 76mm vertical pipe downstream a bend for air velocities between 10.3 to 33.9 m/s, where the latter velocity is in the churn-annular transition region. The experimental arrangement used a WMS sensor one meter downstream of the bend. Four different types of meshes have been used including coarser and finer butterfly mesh, explained in Chapter 5, and an unstructured mesh. The results of void fraction time series for the CFD model used, Eulerian-Eulerian multifluid VOF, has been compared to WMS void fraction results. The authors observed that the time series averaged void fraction fluctuations exhibit a wide range of amplitudes at lower superficial velocities, while these were more uniform at higher superficial velocities. The CFD results showed larger fluctuations compare to experimental results. The authors further analyzed these fluctuations by use of video recordings from the experimental stand. At lower air superficial velocities, they observe a cyclic liquid structure, with a falling liquid film being swept by the subsequent liquid waves. At higher superficial velocities, this falling film was not observed. These behaviors could be observed in the animated CFD results. The Authors compared radial average void fraction profile, which was in a very good agreement with the experimental results. The probability density of void fraction showed one peak and a long tail. This is known as a characteristic of the churn flow. The PDF profiles derived from CFD results were in a good match with WMS measured data.

Peña-Monferrer et al. [11] studied air-water bubbly flow using Eulerian-Eulerian model coupled with PBE (Population Balance Equation). The work is one of rare publications, which has discussed constitutive expressions in detail. The expressions for the drag force and non-

drag forces such as lift force, virtual mass force, wall lubrication force and turbulent dispersion force have been discussed. The bubble induced turbulence is added as a source term in the standard k-ε transport equation. The population balance equation takes account of bubble size evolution by a length-based number density functions (NDF) and terms for birth and death of bubbles by coalescence and breakage. In order to compensate for the computationally expensive PBE solution, a quadrature-based moment method, explained in Chapter 4, is used. The moment method gives an approximate solution to the PBE equation. The experimental set uses a 52mm pipe. A butterfly mesh has been used. A brilliant outcome of this publication is a sensitivity analysis of constitutive models for interfacial forces and bubble induced turbulence. These models has been compared to experimental results for the different cases studied.Tocci et al.

Tocci et al. [12] simulated two cases from the previous publications which had used VOF model. The first case was a 50.8mm pipe and air-water churn flow. The second case was 67mm pipe used by Abdulkadir [9], as described earlier. The study used multifluid Eulerian VOF model in the OpenFOAM software. For the first case, the study compares pressure drop obtained from the CFD model with VOF model results and the results from the OLGA software and shows that the multifluid Eulerian l VOF model has the best agreement with experimental results. For the second case, the study shows that this model gives a better match for the void fraction and film thickness comparing to the VOF model.

Zahedi et al. [13] simulated annular air-water flow in a vertical 72.2mm pipe and pipe bend using both VOF and Eulerian-Eulerian multifluid VOF model. They used a very fine mesh with 4 million cells for the VOF case and a relatively coarser mesh with 0.5 million cells for the Eulerian multifluid model. The void fraction and the PDF of void fraction for both models were compared to experimental results from the WMS. The authors found better representation of flow pattern with the VOF model, which may be due to finer grid used for the VOF case. They found out that both models failed to accurately predict particle detachment from the liquid film into the gas core.

Abood et al. [14] visualized air-oil flow patterns in a narrow tube of 24mm using the VOF model. The range of air velocity is between 0.1 to 6 m/s and 0.1 to 0.3 m/s for the oil. The resulting flow patterns show a very good agreement with the experiment. The air bubbles and Tylor bubbles are visualized by the CFD model. The transition from bubbly to slug flow and further to churn and annular flow are captured by the VOF model. The study shows that for small tubes and moderate gas velocities the VOF model can provide a good prediction of two-phase flow patterns.

Adaze et al. [15] used the Eulerian-Eulerian multifluid VOF model to predict critical gas flows corresponding to onset of wall film reversal in the annular flow. A film reversal, an adverse phenomenon in petroleum industry, happens when the velocity of the gas core is not high enough to sweep the wall film upward. Unlike most of the publications, this work has used a two-dimensional axisymmetric grid. The results of CFD simulation were found to be in a good agreement with the experimental measurements. The authors observed that as the velocity of the gas core decreases, the wall film thickness increases and the inner layer of the film starts to descend. The roll over waves generated, drag the liquid upward and an oscillatory film behavior is observed.

2.3 Flow patterns in vertical upward two-phase flow

There is no exact agreement in the literature regarding the type of flow patterns, also called flow regime, and number of different categorized flow patterns. However, majority of

publications agree with these four flow patterns for vertical upward gas-liquid flow: Bubbly, slug, churn and annular. In fact, it is not easy to categorize flow patterns and in transition from one flow pattern to the other, different flow structure may be observed.

At lower gas and liquid superficial velocities, for about $v_{sl} < 0.1 m/s$ and $v_{sg} < 1 m/s$, dispersed bubbles in the continuous liquid phase has been observed. This corresponds to lower void fractions up to about 0.25. Some sources has suggested bubbly flow for the void fraction up to 0.52 [19]. The disagreement is due to the effect of pipe diameter, fluid properties and many other factors, which may affect vertical two-phase flow patterns. For small diameter pipes, some publications has also reported dispersed bubbly flow at low superficial gas velocities and high superficial liquid velocities, $v_{sl} > 1 m/s$. This has not been reported for large pipes, maybe because the requirement of very high flow rates which is difficult to achieve for large pipes.

Higher superficial gas velocities, cause bubbles to coalesce and make larger cap shaped bubbles typically called Taylor bubbles. These bubbles can grow and occupy the whole cross section of the pipe except a thin liquid film in adjacent to the pipe wall. This flow regime is addressed to as slug flow in the literature and in the industry. It is worth mentioning that slugs may also be created when there is a local minimum in the pipe elevation. This is typically called terrain slug [20], while the former is called hydrodynamic slug. For large pipes, the cap-bubbles may not grow to occupy the whole cross section of the pipe and hydrodynamic slugs may never exists; this has been discussed in the flow maps section. It has been observed that as the Tylor bubbles rise upward through the pipe, the wall film falls downward around the Tylor bubbles. The wake region created in the tail of a rising Taylor bubble cause coalescence and entrainment of subsequent small bubbles.

If the superficial gas velocity increases even higher, the gas can tunnel through the liquid, pushing the liquid to the pipe wall. Waves are formed at the interface between the liquid and gas. These swirling waves have a gas core and sweep the liquid film as they rise. A falling liquid film has been observed subsequent to rising of a wave.

At highest gas superficial velocities, a continuous gas column in the center of the pipe is shaped with a distinct boundary between the gas and liquid phases. This is known as the annular flow pattern. Annular flow is characterized with the wall film region and liquid droplets in gas core. These liquid droplets may entrain in the wall film or detach from the wall film and flow upward with the gas core. If the superficial velocities fall under a critical value, the wall film may start to flow downward.

2.4 Flow pattern maps

Prediction of the flow pattern is an essential task in many industries. The proper design of two-phase flow systems substantially rely on the flow pattern predictions. In some applications such as phase separation, a specific flow pattern is desired. During the years, researchers have tried to develop flow pattern maps, but no one has succeeded to draw a general map, which is valid for all diameters, inclinations and fluid properties [20]. All the flow patterns suggested in the literature are based on limited data sets, which cannot cover even the main factors affecting the flow pattern, namely diameter, fluid properties and inclination angel. Another challenge is that sometimes these data sets are not consistent with each other; one work has reported slug flow for a certain pipe diameter and superficial velocities, while some other experimental works reported churn or even annular flow [19]. This is possibly due to measurement and the subjective flow pattern identification technics.

Development of a flow pattern map is based on designating boundaries between different known flow patterns. Close to these boundaries, the uncertainty of flow pattern identification is high. Whereas, away from the boundaries, the majority of flow pattern maps are aligned [21].

Taitel et al. [22] recorded that the transition from bubble to slug flow, due to agglomeration and coalescence of bubbles, occur at void fraction $\alpha = 0.25$ and suggested an equation for the transition boundary based on the slip velocity of bubbles. Mishima & Ishii [23] suggested that the transition from bubbly to slug flow occur at void fraction $\alpha = 0.30$ and suggested an equation for the boundary.

For the transition from bubble to dispersed bubble, Taitel et al. [22] suggested that turbulence would overcome bubble coalescence at high liquid superficial velocities and proposed an equation based on the theory of break-up of immiscible fluids by turbulence forces. However, Mishima & Ishii [23] have not considered bubble and dispersed bubble as two separate flow patterns.

For the transition boundary between slug and churn flow, Taitel et al. [22] proposed an equation based on the entrance length to form stable slugs. For the slug to churn transition, Mishima & Ishii [23] assumed the condition when nose of the following Taylor bubble touches the tail of preceding bubble and due to the wake effect, stable Taylor bubbles could not form. They formulated it mathematically as when the mean void fraction in the whole flow domain reaches the void fraction within the slug-bubble section. Mishima & Ishii [23] suggested two equations for small and large pipes based on liquid film reversal around large bubbles and destruction of large waves.

Figure 2-1 shows a flow pattern map made by Wu et al. [19], based on the transition boundaries discussed above. A data set of 2500 points has been used for the validation of transition boundaries.

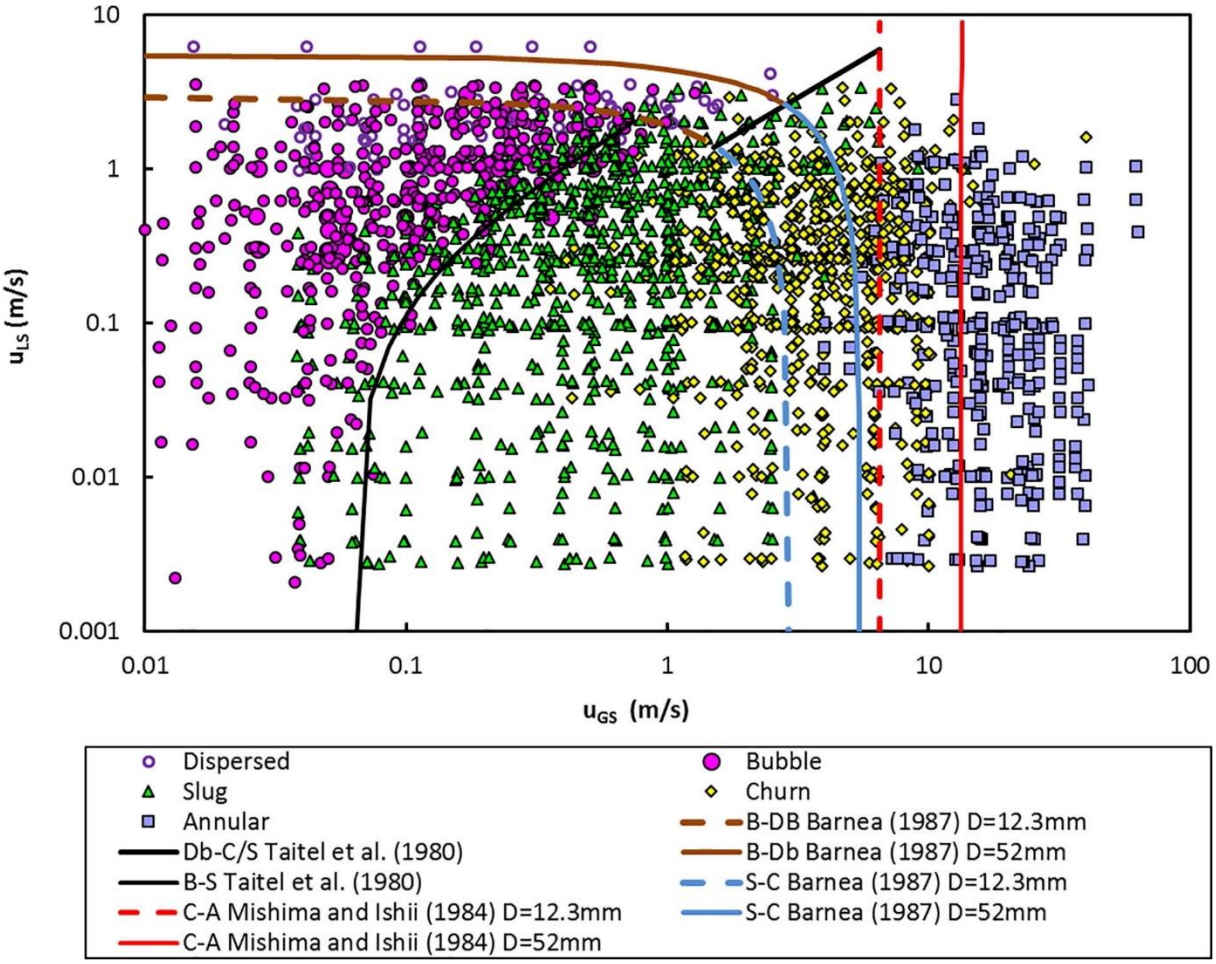

Figure 2-1:Vertical upward flow pattern map suggested by Wu et al. [19]. (B stands for Bubble, D for Dispersed, S for Slug, C for Churn and A for Annular)

Taylor bubble growth in large diameter pipes is limited due to the balance between surface tension and external force. Kataoka & Ishii [1] introduced a critical diameter above which Taylor bubbles cannot occupy the whole cross section of the pipe and the known slug flow pattern could not exist. The critical diameter is defined as:

$$D = 40\sqrt{\frac{\sigma}{g(\rho_l-\rho_g)}} \qquad 2\text{-}1$$

The experiments performed later by Schlegel et al. [24] and Capovilla et al. [25] have confirmed this. The term cap-bubble is used for the flow pattern observed, instead of slug flow pattern.

The majority of experiments for the two-phase vertical upward flow have been performed with water and air as the fluid phases. Experiments performed with other liquids such as oil and glycerol have shown that the fluid properties shift the transition boundaries [19]. Hence, the flow pattern maps based on liquid and gas superficial velocities may not be consistent for other type of fluids. Therefore, researchers have tried to use dimensionless numbers as Froud, Reynolds and Weber numbers. Wu et al. [19] have suggested the flow pattern map shown in Figure 2-1 also based on the gas and liquid Reynolds numbers and Weber numbers.

Barnea [26] modified and improved previous models to a unified model which can be used for all pipe inclinations. Based on Barnea unified model, a computer program called FLOPATN has been developed in the University of Tulsa [27]. Pereyra et al. [21] proposed a general model to quantify the confidence level of two-phase flow pattern prediction. They used FLOPTAN with a data set of 9000 points. They found a general success of 75% for the whole range of data

sets and proposed a transition band based on the dimensionless numbers, instead of sharp transition boundaries. FLOPATN flow pattern map for the case study used in this work is presented in Chapter 5.

2.5 Measuring and identifying flow patterns

Visual inspection has been the fundamental method for identification of the flow patterns. Transparent pipes have mainly been used in the experiments with multiphase flows. For larger pipes, low light penetration into the pipe can cause difficulty in the flow pattern visualization. High speed cameras and in some cases x-ray photography have been used as an alternative for visual inspection.

Instruments for measuring void fraction can be categorized as intrusive and non-intrusive. Intrusive sensors may interfere and affect the flow pattern. The wire mesh sensor (WMS) consists of two layers of fine-wire grid, usually in 16x16, 32x32 construction, placed parallel, close to each other. The number of nodes corresponds to the crossing points of wires. Void fraction is measured based on the conductivity change between the nodes. In this way an instantaneous image of void fraction in the cross section can be achieved.

Unlike WMS, which is an intrusive void fraction measurement, an electrical capacitance tomography (ECT) sensor can provide a non-intrusive void fraction measurement. It is composed of a number of electrodes configured in a circular array. The dielectric permittivity measured between the electrodes, provides an image of void fraction in the cross section. Electrical impedance tomography (EIT) sensor has the same configuration of electrodes as ECT, but the electrodes must be in continuous electrical contact with the electrolyte inside the pipe. An electrical excitation signal is applied through a pair of electrodes. Then electrical responses collected from other electrodes reflects the conductivity distribution in the cross section.

Many other sensors such as gamma densitometer have also been used in experiments but the goal here is just to give a brief introduction to sensors and sensor measurement data.

The instantaneous void fraction measurement for a specific cross section can be obtained by the sensors mentioned above. Figure 2-2 shows typical void fraction read for a cross section of a 150mm pipe using an EIT sensor:

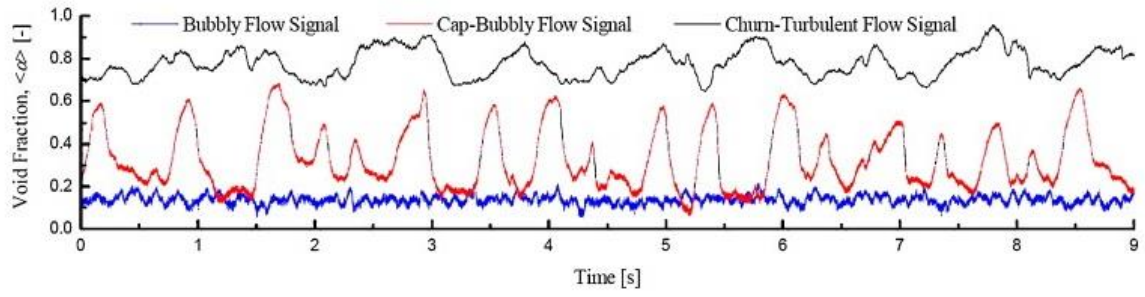

Figure 2-2: Typical shape of measured void fraction signal [24]

An alternative method could be used to obtain the average void fraction in the entire pipe volume. This is achieved by rapid closure of inlet water and air flows and then measuring the volume of water in the test section; for instance by a pressure sensor at the bottom of the test section [25].

Several methods have been used in the literature for objective identifying of the flow pattern. Probability density function (PDF) of void fraction and artificial neural network has been used by majority of researchers. The probability density function of void fraction show a specific shape corresponding to each flow pattern.

For the bubbly and annular flow patterns, the PDF shows a single peak at low and high void fractions respectively. For the slug flow, the PDF displays two peaks, one at lower void fraction and the other at higher void fraction. This results from the nature of slug flow with Taylor bubbles and liquid slugs. For larger pipes, where Taylor bubbles cannot occupy the whole pipe section, the PDF resembles the slug flow PDF with a single peak at lower void fraction. The PDF of churn flow has a single peak at higher void fraction with a broad tail at lower void fractions. Figure 2-3 shows an example of the shape of PDF for void fraction of a small pipe.

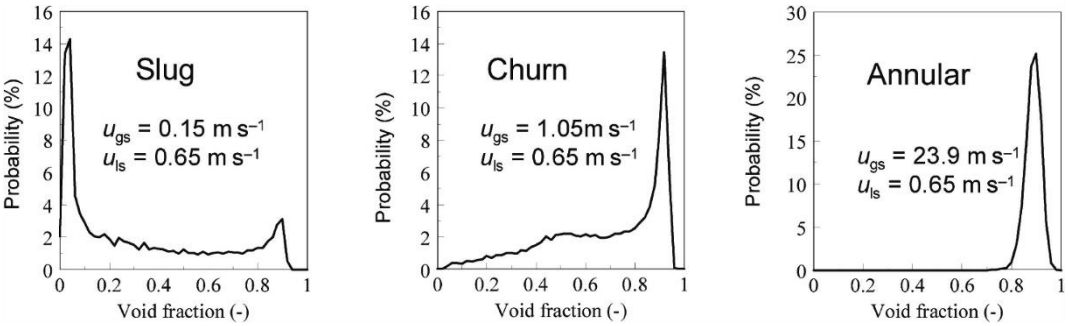

Figure 2-3: PDF of void fraction for different flow patterns of a 5mm diameter pipe [28]

For a large pipe the shape of PDF is relatively the same as a small pipe but since instead of the slug flow, the cap-bubble regime exists, the PDF shows only one peak at lower void fractions and a wide tail, as shown in Figure 2-4:

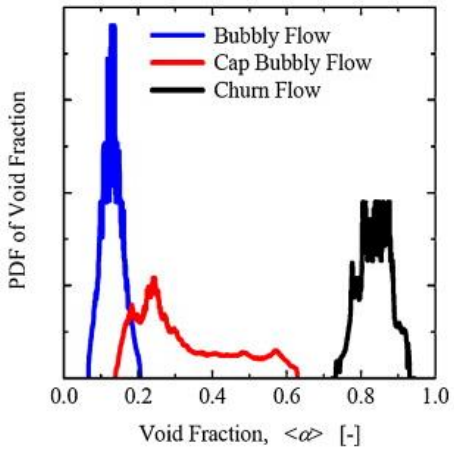

Figure 2-4: The shape of PDF for void fraction for different flow patterns of a 150 mm pipe [24]

3 CFD methods for multiphase flows

This chapter introduces the main CFD approaches used commonly dealing with multiphase flows of gas liquid phases. The models used for solid phases and Lagrangian models are considered out of the scope of this work. It has been tried to introduce the mathematical equations where they were essentially needed in order to show the details of the model. The effort was to use a unified form in introducing equations, where different references use unlike notation and configuration. Equations are presented in their general form; they are not simplified according to the use for the type of task, which is the focus of this work. For example, mass transport terms are not deleted from equations, while mass transfer is not considered in this work.

3.1 Mixture model

The mixture model uses one momentum equation for the mixture by summing the individual momentum equations for all phases. Though, like drift-flux model, an algebraic correlation is used to compute the relative velocity; assuming local equilibrium over short spatial length scales. Equation 3-1 shows the mixture momentum equation [29]

$$\frac{\partial}{\partial t}(\rho_m \vec{v}_m) + \nabla.(\rho_m \vec{v}_m \vec{v}_m) = -\nabla p + \nabla.\left[\mu_m\left(\nabla \vec{v}_m + \nabla \vec{v}_m{}^T\right)\right] + \rho_m \vec{g} + \vec{F} + \nabla.\left(\sum_{k=1}^{n} \alpha_k \rho_k \vec{v}_{dr,k} \vec{v}_{dr,k}\right) \quad 3\text{-}1$$

Where, ρ_m and μ_m are mixture density and viscosities, defined as:

$$\rho_m = \sum_{p=1}^{n} \alpha_p \rho_p \quad 3\text{-}2$$

$$\mu_m = \sum_{k=1}^{n} \alpha_p p \quad 3\text{-}3$$

$\vec{v}_{dr,p}$ is the drift velocity for the secondary phase p, defined as:

$$\vec{v}_{dr,p} = \vec{v}_p - \vec{v}_m \quad 3\text{-}4$$

The mixture model could be used as homogeneous model by unchecking the slip velocity option. In this case, the velocity field is the same for all phases. ANSYS Fluent uses Manninen [30], slip velocity formulation but it is also possible to use other correlations by user defined functions UDFs.

The mixture model could be effectively used for prediction of void fraction and pressure drop, when the dispersed phase is a dilute phase. However, this model cannot predict the flow pattern.

3.2 Volume of Fluid Model

The Volume of Fluid (VOF) model is a surface tracking method between two or more non-mixable fluids. The VOF model uses a single momentum equation for all phases, hence the velocities of phases are assumed equal. The VOF model basically tracks the volume fraction of each phase in each computational cell throughout the Eulerian domain.

In the VOF approach the general form of the continuity equation for each secondary phase (p) is [29]:

$$\frac{1}{\rho_q}\left[\frac{\partial}{\partial t}(\alpha_q \rho_q) + \nabla.\left(\alpha_q \rho_q \overrightarrow{v_q}\right)\right] = S_{\alpha_q} + \sum_{p=1}^{n}(\dot{m}_{pq} - \dot{m}_{qp}) \quad 3\text{-}5$$

The first term on the right hand side of the above question is the source term and the second term accounts for mass transfer between phases p and q.

Then, the volume fraction of the primary phase would be derived from:

$$\sum_{q=1}^{n} \alpha_q = 1 \qquad 3\text{-}6$$

As mentioned above the VOF model solves one momentum equation for all phases:

$$\frac{\partial}{\partial t}(\rho\vec{v}) + \nabla.(\rho\vec{v}\vec{v}) = -\nabla p + \nabla.[\mu(\nabla\vec{v} + \nabla\vec{v}^T)] + \rho\vec{g} + \vec{F} \qquad 3\text{-}7$$

This is the main limitation of VOF model as it fails to find the slip velocity between the phases and leads to inaccurate results when the velocity difference between phases is large. However, this model has shown good results for small diameter pipes at low velocities. This model is capable of predicting the flow pattern by tracking the interface between phases.

3.3 Eulerian model

The Eulerian model solves a separate set of continuity and momentum equation for each phase. The form of continuity equation is the same as discussed for the VOF model. The momentum balance for each phase q is [29]:

$$\frac{\partial}{\partial t}(\alpha_q\rho_q\vec{v}_q) + \nabla.(\alpha_q\rho_q\vec{v}_q\vec{v}_q) = -\alpha_q\nabla p + \nabla.\bar{\bar{\tau}}_q + \alpha_q\rho_q\vec{g} + \sum_{p=1}^{n}(\vec{R}_{pq} + \dot{m}_{pq}\vec{v}_{pq} - \dot{m}_{qp}\vec{v}_{qp}) + (\vec{F}_q + \vec{F}_{lift,q} + \vec{F}_{wl,q} + \vec{F}_{vm,q} + \vec{F}_{td,q}) \qquad 3\text{-}8$$

The last group on the RHS of momentum equation, usually called non-drag forces, are the body force, lift force, wall lubrication force and turbulent dispersion force respectively. These are explained later in this chapter.

The interphase force $\vec{R}_{pq}$ is defined as:

$$\sum_{p=1}^{n}\vec{R}_{pq} = \sum_{p=1}^{n}K_{pq}(\vec{v}_p - \vec{v}_q) \qquad 3\text{-}9$$

This term is generally called drag force in the literature. Though, there is no uniform formulation for the drag force in the literature. K_{pq} is called the interphase momentum exchange coefficient. Commonly, the drag force in the literature is defined based on the flow regime. For the spherical bubbles of uniform size, Ishii & Mishima [31] defined the drag force as:

$$\vec{R}_{pq} = \frac{3}{4}\alpha_p\frac{C_D\rho_p}{d_p}|\vec{v}_p - \vec{v}_q|(\vec{v}_p - \vec{v}_q) \qquad 3\text{-}10$$

For bubbly, slug or churn flows, this can be modified based on the interfacial area concentration [32]:

$$\vec{R}_{pq} = \frac{1}{8}C_D A_p\rho_p|\vec{v}_p - \vec{v}_q|(\vec{v}_p - \vec{v}_q) \qquad 3\text{-}11$$

ANSYS Fluent [29] uses a different formulation for the fluid-fluid exchange coefficient based on the interfacial area:

$$K_{pq} = \frac{\rho_p f}{6\tau_p}d_p A_p \qquad 3\text{-}12$$

$$\tau_p = \frac{\rho_p {d_p}^2}{18\mu_q} \qquad 3\text{-}13$$

Where, τ_p is the particle (bubble or droplet) relaxation time. f is a function based on the drag coefficient C_D and the Reynolds number. Ansys Fluent provides several drag functions. The drag function is normally in the form of:

$$f = \frac{C_D Re}{24} \qquad 3\text{-}14$$

Where the Reynolds number in equation 3-14 is defined as:

$$Re = \frac{\rho_q|\vec{v}_p - \vec{v}_q|d_p}{\mu_q} \qquad 3\text{-}15$$

The interfacial area is obtained either by a transfer equation or by a correlation; explained later in this chapter.

There are variety of drag coefficient C_D, models in the literature. Some of these models are available in the ANSYS Fluent. It is also possible to introduce a customized drag model through UDFs.

Anisotropic drag law in ANSYS Fluent uses a higher drag force in the normal direction to the interface comparing to the tangential direction based on an anisotropy ratio.

3.3.1 Granular phase

In the case that the dispersed phase is a granular solid, ANSYS Fluent provides application of the kinetic theory of granular flow in an Eulerian framework. This has not been discussed here, as considering out of the scope of this study.

3.4 Turbulence modeling

Direct numerical simulation (DNS) of the Navier-Stokes equations requires an extreme fine grid and minor time step to resolve the smallest turbulent eddies and the fastest fluctuations, which is not possible for engineering applications. The alternative is even time filtering or spatial filtering of the flow equations or a mixture of both. Large eddy simulation (LES) uses a spatial filtering to separate larger and smaller eddies and solves filtered flow equations. Instead, Reynolds averaged Navier-Stokes simulation (RANS) is based on Reynolds (ensemble) averaging, where each flow variable is a sum of a time averaged and a fluctuating component ($\emptyset = \overline{\emptyset} + \acute{\emptyset}$). By substituting this into the instantaneous continuity and momentum equations, extra shear stresses called Reynolds stresses appear in the momentum equation.

Reynolds stress (RSM) model uses one transfer equation for each of Reynolds stress terms. Alternatively, the Boussinesq hypothesis relates the Reynolds stresses to the mean velocity gradients by turbulent viscosity. The two most used turbulence models, $k-\varepsilon$ and $k-\omega$ use this approach. The $k-\varepsilon$ turbulence model has been presented here, since it has been used in this study.

The turbulent viscosity and two transfer functions for k and ε are [29]:

$$\mu_t = \rho C_\mu \frac{k^2}{\varepsilon} \qquad 3\text{-}16$$

$$\frac{\partial}{\partial t}(\rho k) + \nabla.(\rho k \vec{v}) = \nabla.\left[\left(\mu + \frac{\mu_t}{\sigma_k}\right)\nabla k\right] + G_k + G_b - \rho\varepsilon - Y_M + S_k \qquad 3\text{-}17$$

$$\frac{\partial}{\partial t}(\rho \varepsilon) + \nabla.(\rho \varepsilon \vec{v}) = \nabla.\left[\left(\mu + \frac{\mu_t}{\sigma_\varepsilon}\right)\nabla \varepsilon\right] + C_{1\varepsilon}\frac{\varepsilon}{k}(G_k + C_{3\varepsilon}G_b) - C_{2\varepsilon}\rho\frac{\varepsilon^2}{k} + S_\varepsilon \qquad 3\text{-}18$$

Where, G_k represents the generation of turbulence kinetic energy due to the mean velocity gradients, G_b is the generation of turbulence kinetic energy due to buoyancy and Y_M contributes to the fluctuating dilatation in compressible turbulence to the overall dissipation rate [29].

$C_{1\varepsilon}$, $C_{2\varepsilon}$ and $C_{3\varepsilon}$ are constants and σ_k and σ_ε are the turbulent Prandtl numbers for k and ε.

S_k and S_ε are user-defined source terms.

3.4.1.1 RNG k-ε Model

Comparing to standard *k-ε* model, the RNG *k-ε* provides a more accurate and reliable turbulence model for a wider class of flows; including rapidly strained, swirl and low-Reynolds flows [29]. The model is derived from the Navier-Stokes equations using a mathematical technique

called "renormalization group" (RNG) methods. The transfer function and the constants are slightly different from the standard *k-ε* model explained above. The transfer functions for *k* and *ε* are:

$$\frac{\partial}{\partial t}(\rho k) + \nabla.(\rho k \vec{v}) = \nabla.\left[\alpha_k \mu_{ef} \nabla k\right] + G_k + G_b - \rho\varepsilon - Y_M + S_k \quad 3\text{-}19$$

$$\frac{\partial}{\partial t}(\rho \varepsilon) + \nabla.(\rho \varepsilon \vec{v}) = \nabla.\left[\alpha_k \mu_{ef} \nabla \varepsilon\right] + C_{1\varepsilon}\frac{\varepsilon}{k}(G_k + C_{3\varepsilon}G_b) - C_{2\varepsilon}\rho\frac{\varepsilon^2}{k} - R_\varepsilon + S_\varepsilon \quad 3\text{-}20$$

The effective viscosity μ_{ef} in equations 3-19 and 3-20 is derived from the following equation:

$$d\left(\frac{\rho^2 k}{\sqrt{\varepsilon\mu}}\right) = 1.72\frac{\hat{v}}{\sqrt{\hat{v}^3 - 1 + C_v}}d\hat{v} \quad 3\text{-}21$$

Where, $\hat{v} = \frac{\mu_{eff}}{\mu}$ 3-22

and $C_v \approx 100$.

3.4.1.2 Scalable wall functions

A major problem with standard wall functions is the requirement for the grid near the wall region. To model the wall shear stress correctly, it is required that the first cell to be located in the log-layer, which typically requires that $30 < y^+ < 300$. This requirement opposes difficulty in generating the grid. It requires a coarser mesh close to the wall to ensure the y^+ requirement. The use of scalable wall functions relax this constraint and a grid with arbitrary refinement can be used [29].

Troshko & Hassan [33] studied different logarithmic wall laws for multiphase bubbly flows and suggested a proportionality coefficient accounting for high void non-linearity. This was correlated as function of friction velocity and resulted in better agreement with the experiment. Majority of publications discussed in Chapter 2 have used standard wall laws.

3.4.1.3 Turbulence in multiphase flows

There are basically three approaches in modeling of turbulence for multiphase flows. When the secondary phase is a dispersed dilute phase, a modified *k-ε* model could be used for the primary phase q [29]:

$$\frac{\partial}{\partial t}(\alpha_q \rho_q k_q) + \nabla.(\alpha_q \rho_q k_q \vec{v}_q) = \nabla.\left[\alpha_q\left(\mu_q + \frac{\mu_{t,q}}{\sigma_k}\right)\nabla k_q\right] + \alpha_q G_{k,q} - \alpha_q \rho_q \varepsilon_q + \alpha_q \rho_q \Pi_{kq} \quad 3\text{-}23$$

$$\frac{\partial}{\partial t}(\alpha_q \rho_q \varepsilon_q) + \nabla.(\alpha_q \rho_q \varepsilon_q \vec{v}_q) = \nabla.\left[\alpha_q\left(\mu_q + \frac{\mu_{t,q}}{\sigma_k}\right)\nabla \varepsilon_q\right] + \alpha_q \frac{\varepsilon_q}{k_q}(C_{1\varepsilon}G_{k,q} - C_{2\varepsilon}\rho_q \varepsilon_q) + \alpha_q \rho_q \Pi_{\varepsilon q} \quad 3\text{-}24$$

The effect of turbulence for the dispersed phase p, are not obtained from transport equations, but through the source terms Π_{kq} and $\Pi_{\varepsilon q}$.

In the mixture turbulence model, like the homogeneous model, phase mixture velocity $\vec{v}_m$, density ρ_m and viscosity μ_m are used and a single transfer function for the *k* and *ε* of the mixture would be solved.

The most complete turbulence model uses a single pair of *k-ε* transfer equations for each phase. This is more computationally expensive but can capture turbulence transfer among the phases more precisely. The transfer functions for *k* and *ε* in this approach are [29]:

$$\frac{\partial}{\partial t}(\alpha_q \rho_q k_q) + \nabla.(\alpha_q \rho_q k_q \vec{v}_q) = \nabla.\left[\alpha_q\left(\mu_q + \frac{\mu_{t,q}}{\sigma_k}\right)\nabla k_q\right] + \alpha_q G_{k,q} - \alpha_q \rho_q \varepsilon_q + \sum_{p=1}^{n} K_{pq}(C_{pq}k_p - C_{qp}k_q) - \sum_{p=1}^{n} K_{pq}(\vec{v}_p - \vec{v}_q).\frac{\mu_{t,p}}{\alpha_p \sigma_p}\nabla \alpha_p + \sum_{p=1}^{n} K_{pq}(\vec{v}_p - \vec{v}_q).\frac{\mu_{t,q}}{\alpha_q \sigma_q}\nabla \alpha_q + \Pi_{kq} \quad 3\text{-}25$$

$$\frac{\partial}{\partial t}(\alpha_q \rho_q \varepsilon_q) + \nabla.(\alpha_q \rho_q \varepsilon_q \vec{v}_q) = \nabla.\left[\alpha_q\left(\mu_q + \frac{\mu_{t,q}}{\sigma_k}\right)\nabla\varepsilon_q\right] + \frac{\varepsilon_q}{k_q}\Big[C_{1\varepsilon}\alpha_q G_{k,q} - C_{2\varepsilon}\alpha_q \rho_q \varepsilon_q +$$
$$C_{3\varepsilon}\left(\sum_{p=1}^{n} K_{pq}(C_{pq}k_p - C_{qp}k_q) - \sum_{p=1}^{n} K_{pq}(\vec{v}_p - \vec{v}_q).\frac{\mu_{t,p}}{\alpha_p \sigma_p}\nabla\alpha_p + \sum_{p=1}^{n} K_{pq}(\vec{v}_p - \vec{v}_q).\frac{\mu_{t,q}}{\alpha_q \sigma_q}\nabla\alpha_q\right)\Big] + \Pi_{\varepsilon q} \quad 3\text{-}26$$

The source terms Π_{kq} and $\Pi_{\varepsilon q}$ in the above equations could be used to model turbulence interactions. ANSYS Fluent provides several models for turbulence interaction. The turbulence interaction may be neglected, but in some flows, it has an important role.

3.5 Lift force

The experiments performed in the 80s and 90s showed that small bubbles tend to migrate to channel wall, while large bubble tend to migrate to the center [34]. The lateral force on the bubbles or droplets of dispersed phase due to velocity gradients in the continuous phase is known as the lift force in multiphase flow modeling.

The lift force may be neglected in some flows, but it could be important in some cases, especially when there is a high slip velocity. ANSYS Fluent uses the common formulation used in the literature. The lift force experienced by the dispersed phase p in a continuous phase q, is based on the slip velocity and local vorticity of the continuous phase (curl of the velocity vector):

$$\vec{F}_{lift} = -C_l \rho_q \alpha_p (\vec{v}_q - \vec{v}_p) \times (\nabla \times \vec{v}_q) \quad 3\text{-}27$$

ANSYS Fluent provides several models for computing the lift coefficient C_l.

3.6 Wall lubrication force

The wall lubrication force also known as the wall lift force, exerts another lateral force than the lift force on the dispersed phase (bubbles) due to surface tension. The name comes from the analogy that the force prevent bubbles from attaching the wall and acts like a lubrication force.

The common formulation of the wall lubrication force experienced by the dispersed phase p in a continuous phase q is as:

$$\vec{F}_{wl} = C_{wl}\rho_q \alpha_p \left|(\vec{v}_q - \vec{v}_p)_{||}\right|^2 \vec{n}_w \quad 3\text{-}28$$

$(\vec{v}_q - \vec{v}_p)_{||}$ in equation 3-28 is the tangential component of the slip velocity and $\vec{n}_w$ is the wall unit normal vector.

ANSYS Fluent provides several models for the wall lubrication coefficient, C_{wl}.

3.7 Virtual mass force

When the secondary phase p accelerates relating to the primary phase q, it exerts a force on the primary phase as a result of accelerating the boundary layer around the bubble/droplet and at the same time pushing the primary phase aside. The virtual mass force is defined as:

$$\vec{F}_{wm} = C_{vm}\rho_q \alpha_p \left(\frac{D\vec{v}_q}{Dt} - \frac{D\vec{v}_p}{Dt}\right) \quad 3\text{-}29$$

A virtual mass coefficient value of 0.5 is commonly used in the literature, which is derived based on the potential flow theory around a spherical bubble [11].

3.8 Turbulent dispersion force

Turbulent dispersion force is the force experienced by the dispersed phase p due to the turbulence in the continuous phase q. In gas liquid flows, this appears as the bubble motion induced by liquid phase turbulent energy. The averaged multi-phase continuity equations do not include a phasic diffusion effect [34], adding this force to the momentum equation can compensate for that. However, ANSYS Fluent has the option to include turbulent dispersion term in the governing equations of phase volume fractions [29]. Alternatively, models of turbulent dispersion force could be used. Lopez de Bertodano Model [35] is based on the turbulent kinetic energy k_q and the gradient of dispersed phase volume fraction $\nabla\alpha_p$:

$$\vec{F}_{td,q} = -\vec{F}_{td,p} = C_{TD}\rho_q k_q \nabla\alpha_p \qquad 3\text{-}30$$

There is another common formulation in the literature, which uses drag coefficient [32].

3.9 Interfacial area concentration

The exchange of mass, momentum and energy between the phases occurs through the interface between the phases. The interfacial area between two phases is defined as the interfacial area concentration. The interfacial transfer of mass, momentum and energy are proportional to the interfacial area concentration and a driving force. The transfer rates are computed from the product of the interfacial flux and the interfacial area [34]. Hence, the interfacial area concentration model could have significant effect on the CFD simulation of multiphase flows.

Another important aspect of interfacial area model is when the population balance model is not used to account for the size and distribution of the discrete phase. Then, the interfacial area equation takes care of growth, expansion, coalescence, breakage and other mechanisms involved in modeling of particles, droplets or bubbles. In a way, interfacial area transfer equation is a simplification of the population balance equation [36].

Interfacial correlations can be used where the significance of size and distribution of bubbles or droplets do not justify the computational expense of solving an extra transfer equation. These correlations are a relationship between a constant bubble/droplet diameter and the interfacial area concentration. For a spherical bubble or droplet:

$$A_p = \frac{\pi {d_b}^2}{\frac{1}{6}\pi {d_b}^3} = \frac{6}{d_b} \qquad 3\text{-}31$$

The ANSYS Fluent symmetric model is defined as [29]:

$$A_p = \frac{6\alpha_g(1-\alpha_g)}{d_b} \qquad 3\text{-}32$$

In equation 3-32, A_p is the interfacial area concentration and α_g is the gas phase volume fraction.

The interfacial area concentration transfer equation is defined as [29]:

$$\frac{\partial(\rho_g A_p)}{\partial t} + \nabla.\left(\rho_g \vec{u}_g A_p\right) = \frac{1}{3}\frac{D\rho_g}{Dt}A_p + \frac{2}{3}\frac{\dot{m}_g}{\alpha_g}A_p + \rho_g(S_{RC} + S_{WE} + S_{TI}) \qquad 3\text{-}33$$

The first term on the RHS of the above equation represents compressibility effect on the area of gas bubbles and the second term represents the mass transfer effect. Please note that neither compressibility nor mass transfer are considered in this study.

The source term S_{RC} in equation 3-33 accounts for random collision driven by turbulence.

The source term S_{WE} accounts for wake entrainment coalescence, resulting from acceleration of the bubbles in tail wake of the preceding bubble.

The source term S_{TI} accounts for impact of turbulent eddies on break-up of bubbles

Figure 3-1 and Figure 2-1show these mechanisms in the bubbly flow:

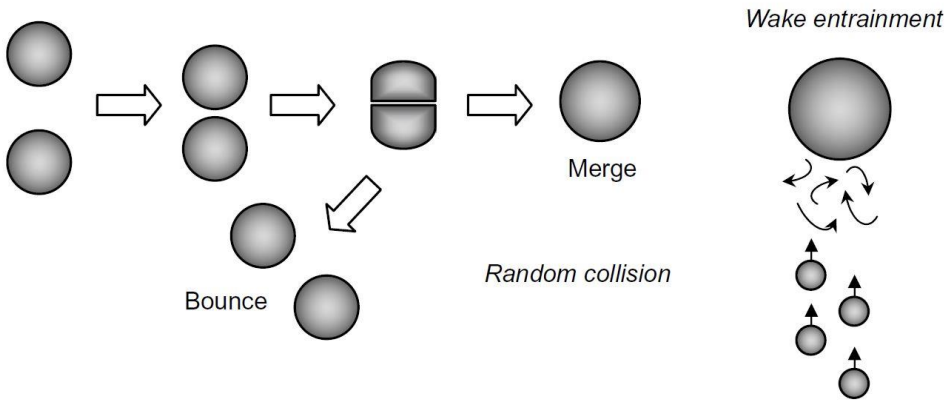

Figure 3-1: Bubble collision and entrainment in a wake of larger rising bubble [32]

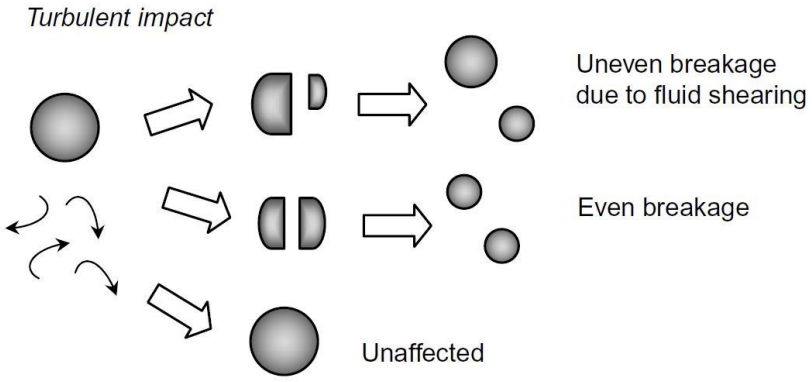

Figure 3-2: Possible impacts of turbulent eddies on bubbles [32]

ANSYS Fluent provides three different models for these source terms: Hibiki & Ishii [37], Ishii & Kim [38] and Yao & Morel [39] model. The first two models where developed based on bubbly flow while the latter one is mainly developed for nucleation boiling application.

3.9.1.1 Bubble/droplet size

The available models in ANSYS Fluent for the source terms in the interfacial area concentration transfer equation, are based on a single average scalar approach. This means that the bubble size distribution is assumed constant or a mean diameter is used. Sauter mean diameter, which accounts for both volume and surface area can be used for averaging. Hence, The Sauter mean diameter and the interfacial area concentration are essentially interconnected. Hibiki & Ishii [37] define Sauter diameter as:

$$d_b = \frac{6A_p}{\alpha_g} \qquad 3\text{-}34$$

There are other single average scalar approach models available in the literature, which can be applied by using UDFs. Schlegel et al. [40] introduced a model for large pipes, since the Hibiki & Ishii [17] model is based on data fitting for small sized pipes. The multiple bubble size approach has been discussed briefly in the population balance section.

Another challenge with single average scalar approach is that these models are generally developed for bubble flow with the assumption that bubbles has spherical form. For other flow patterns, where bubble could be cap shaped or in other forms, the single average scalar approach may not be precise.

3.10 Population balance equation

The population balance of particles in a system is a measure of number of particles in that system. For the gas liquid systems, these particles could be bubbles or droplets. In an Eulerian framework, the number of these particles (droplet or bubbles) dynamically depends on the birth and death phenomena of these particles. The state of the particles is defined by the internal and external coordinates. The external coordinates specifies the position of particles in the flow domain at each time. While, the internal coordinate specifies internal properties of particles such as particle size and temperature. Figure 3-3 depicts these two definitions for the case particles are bubbles:

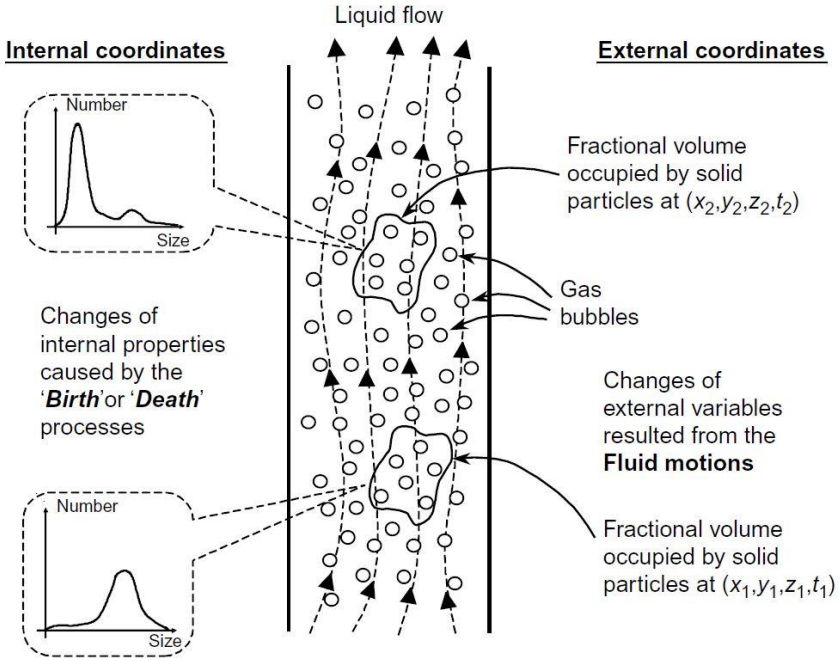

Figure 3-3: Internal and external coordinates of particles (bubbles in this case) [32]

Based on this, the population balance equation (PBE) could be presented as shown in equation 3-35.

$$\frac{\partial f(\vec{x},\emptyset,t)}{\partial t} + \nabla.\left(\vec{v} f(\vec{x},\emptyset,t)\right) = S(\vec{x},\emptyset,t) \qquad 3\text{-}35$$

Where, $f(\vec{x},\emptyset,t)$ is the particle size distribution (PSD); $\emptyset$ is the internal coordinate which could be volume or diameter of particles for example, and $S(\vec{x},\emptyset,t)$ is the source term due to coalescence and breakup phenomena.

The source term could be defined as [39]:

$$S(\vec{x},\emptyset,t) = \frac{1}{2}\int_0^{\emptyset} a(\emptyset-\acute{\emptyset},\acute{\emptyset})f(\emptyset-\acute{\emptyset},t)f(\acute{\emptyset},t)d\acute{\emptyset} - f(\emptyset,t)\int_0^{\infty} a(\emptyset,\acute{\emptyset})f(\acute{\emptyset},t)d\acute{\emptyset} + \int_{\emptyset}^{\infty}\gamma(\acute{\emptyset})b(\acute{\emptyset},\emptyset)p(\acute{\emptyset},\emptyset)f(\acute{\emptyset},t)d\acute{\emptyset} - b(\acute{\emptyset},\emptyset)f(\emptyset,t) \quad 3\text{-}36$$

The first term on the RHS of equation 3-36 defines birth due to coalescence, the second term defines death due to coalescence, the fourth term defines birth due to breakup and the last term defines death due to breakup. $a(\emptyset-\acute{\emptyset},\acute{\emptyset})$ is the coalescences rate between particle of size $\emptyset$ and $\acute{\emptyset}$. $b(\acute{\emptyset},\emptyset)$ is the breakup rate of particle of size $\emptyset$ into $\acute{\emptyset}$. $\gamma(\acute{\emptyset})$ is the number of particles generated from the breakup of particles of size $\acute{\emptyset}$. $p(\acute{\emptyset},\emptyset)$ is the possibility density function (PDF) of breakup of particles with size $\acute{\emptyset}$.

Computation of the population balance equation is dramatically expensive. Yet, due to its practical use, some methods, such as Monte Carlo methods, method of moments (MOM) and class methods (CM), have been introduced for simplifying computation of this equation.

In the MOM method, the *k*-order moment of a particle size distribution, PSD is defined as:

$$m^k(\vec{x},t) = \int_0^{\infty} f(\vec{x},\emptyset,t)\emptyset^k d\emptyset \quad 3\text{-}37$$

The first few moments are then often used for estimating population of particle properties. This method reduces the computational effort for solving PBE significantly.

In the Quadrature Method of Moments (QMOM), the PSD is approximated by a finite set of Dirac's delta functions:

$$f(\vec{x},\emptyset,t) \approx \sum_{i=1}^{N} N_i(\vec{x},t)\delta(\emptyset-\emptyset_i(\vec{x},t)) \quad 3\text{-}38$$

Where N_i is the "weight" or number density of the *i*th class.

A simple approach to the Population balance equation is the average quantities approach, where an average number density for all particles is used. The interfacial area concentration, IAC, which presented in section 3.9, is based on this approach.

4 Task & Methodology

The main approaches in CFD for dealing with multiphase flows have been discussed in Chapter 3. Chapter 2 also reviewed publications, which have used different combinations of these methods for different flow regimes in a vertical gas-liquid upward flow. With this background, this chapter will proceed by defining the task and the CFD model suggested for solving this task.

4.1 Assumptions

In defining and solving the case study introduced later in this chapter, following assumptions have been made:

- The temperature change effects are not considered. The energy equation has not been solved for the task based on the adiabatic assumption.
- Mass transport between the phases is not considered. In many two-phase gas-liquid flows, mass transfer could have an important role. For the air-water system considered in this task, mass transfer is not a matter of concern.
- Compressibility effect for gas phase is not considered. For the minor pressure changes in this task, compressibility is not significant. However, in many gas-liquid flows this could be very important.
- Pressure field is considered the same for both phases. In some gas liquid flows, there is a difference in pressure between the phases.

4.2 The experimental case

There are relatively broad range of publications reporting experimental results for the vertical two-phase upward flow. Majority of these publications are focused on a specific flow pattern. Another problem is that most of the experiments performed for small-bore pipes. This work is interested in process engineering application of two-phase flows where small tubes are not generally used. As discussed in Chapter 2, the effect of diameter is quite significant for the flow pattern type. Another problem is that many of the publications have not reported all the data required, as for example the pressure gradient.

Capovilla et al. [25] have recently performed a broad range of experiments for larger pipes. Experiments presented by them involve three pipe diameters of 97mm, 199mm and 297mm. The 97mm pipe covered a broader range of gas superficial velocities. The 97 mm pipe has therefore been chosen as the experimental case for verifying the CFD results in this study. Besides, the number of computational cells for larger pipes could make the task challenging regarding computational time.

Figure 4-1 shows the experimental setup for the 97mm pipe which has been used as the reference for verification of simulation results.

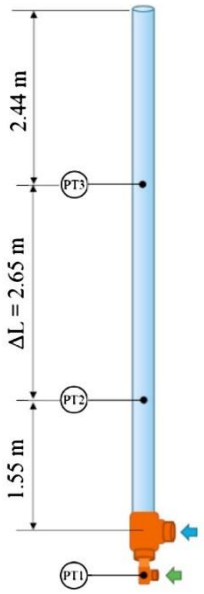

Figure 4-1: Experimental setup for 97mm pipe used by Capovilla et al. [25]

4.3 Defining the task

4.3.1 Simulation cases

The seven cases defined for CFD simulations are based on the experimental work performed by Capovilla et al. [25]. The intension was to choose an experimental basis for verification of CFD results with a broad range of flow pattern and gas superficial velocities. The seven cases presented cover the range of flow patterns from the onset of bubble to cap-bubble/slug to the onset of churn to annular flow regime. This enables tracking the changes in the flow pattern observed from the CFD results and the experimental reported flow pattern. The cases are shown in flow pattern maps in Chapter 5.

4.3.2 Phase fluid properties

Table 4-1 shows the properties of each phase used in CFD simulations.

Table 4-1: Phase fluid properties

Property	Unit	Liquid	Gas
Density	$\frac{kg}{m^3}$	998.2	1.225
Viscosity	$Pa \cdot s$	0.001003	1.7894E-5
Surface tension	$\frac{N}{m}$	0.072	

The properties of water and air used in the experimental reference may deviate from these values, but it was unfortunately not reported. However, since this deviation is minor, the effects on the results are assumed negligible.

4.3.3 Geometry

During primary simulations of the task, it was noticed that the inlet section could affect the results by changing the required length for the so-called fully developed two-phase flow regime. It was experienced that changing the inlet direction and form, also could make convergence of the flow field more difficult. It was found that adding horizontal sections to the main vertical study section would give smooth changing of the flow after the bend and fully developed vertical two-phase flow pattern were reached shortly after the bend. The vertical section is 4 meters, about 41 times diameter; which was observed to be adequate. The geometry is presented in Figure 4-2:

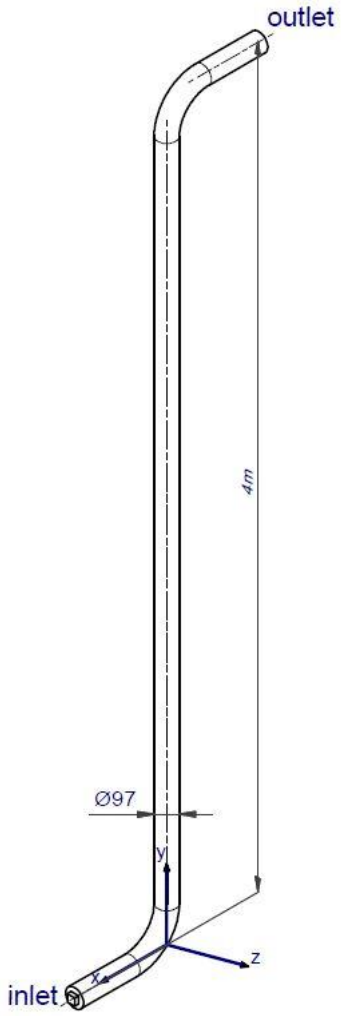

Figure 4-2: The geometry used for the task

4.4 Mesh

After defining and modeling the geometry, the first step in solving a CFD problem is generating the grid. Generating the mesh is not always straightforward and the type and quality of the mesh affects both convergence of the equations solved and the accuracy of the results obtained. An unnecessary fine mesh results in a long computational time, while a coarse mesh may result in divergence or inaccurate results.

For a three-dimensional geometry, the types of cells to be used are hexahedral, tetrahedral, pyramid, wedge, and polyhedral. There are a couple of quantitive factors for mesh quality.

Orthogonal quality in a cell is the dot product of each face normal vector and the normal vector from the centroid of the cell to the centroid of that face. **Orthogonal skewness** is the dot product of the normal vector from the centroid of the cell to the centroid of that face and the normal vector of the adjacent face. **Aspect ratio** is defined as the ratio of the maximum value of the normal distance between the cell centroid and face centroids and the minimum value of the distances between the cell centroid and the corresponding nodes. Generally, when the quality of the mesh is higher, the flow could be more aligned with the mesh and the numerical diffusion is reduced.

Tetrahedral dominant grids have generally less quality comparing to hexahedral grids and are mainly used when the geometry is complex and does not allow using hexahedral dominant grid. A structured mesh uses a uniform pattern mainly made of hexahedral cells. The geometry used for this task is relatively simple and hexahedral cells could be effectively used.

Hernandez-Perez et al. [42] verified several different types of structured and unstructured mesh types for a task of vertical two-phase upward flow. The study concluded that a certain type of mesh called butterfly mesh, Figure 4-3, yields a better convergence and computational time. A mesh sensitivity evaluation, sometimes referred as mesh independence assessment, aims to find the proper grid for the specific problem which quality does not affect the results. Parsi et al. [10] have also verified different types of grids and adopted butterfly mesh as the optimum grid for the task of vertical two-phase flow. They also performed a sensitivity evaluation for the butterfly grid used. Based on this, this study has also adopted a butterfly grid. A cross section of the mesh is shown in Figure 4-3.

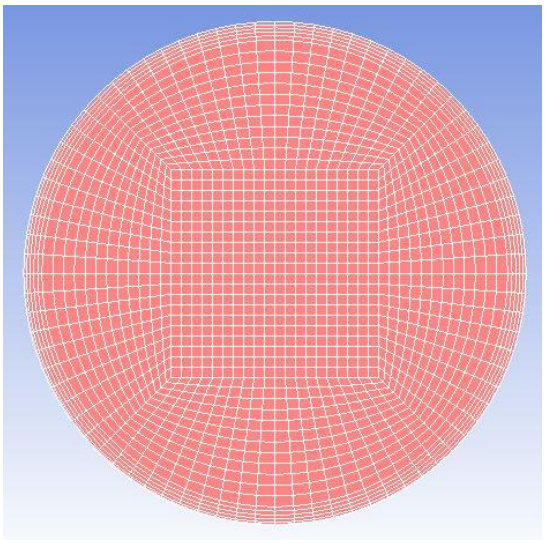

Figure 4-3: Cross section of the mesh used

This cross section has been swept through the whole domain. As it can be seen from the Figure 4-3, five layers of inflation are used close to the wall. This is intended to capture the near wall flow and the wall film. As discussed in Chapter 3, scalable wall functions are insensitive to the position of the first cell close to the wall and this allows the finer mesh close to the wall. For the broad range of cases used in this study, and a long computational time involved, a sensitivity analysis was not practical. Hence, a fine-resolution mesh, comparing to the studies reviewed in Chapter 2, was used. The total number of cells for the whole computational domain are 1106320.

4.5 Boundary conditions

The boundary condition used for the **inlet** is "velocity inlet". Separate inlets have been used for the air and water. The air has been injected from the square section in the center of the pipe, as shown in Figure 4-4. The reason for this section being rectangular is just because it simplifies the creation of the mesh. Water has been injected from the rest of pipe cross section, as shown in the Figure 4-4 . The velocity value for each inlet is then scaled based on the area of the inlet and superficial velocity in the pipe:

$$v_{inlet,g} = v_{sg} \frac{A}{A_{inlet,g}} \quad 4\text{-}1$$

$$v_{inlet,l} = v_{sl} \frac{A}{A_{inlet,l}} \quad 4\text{-}2$$

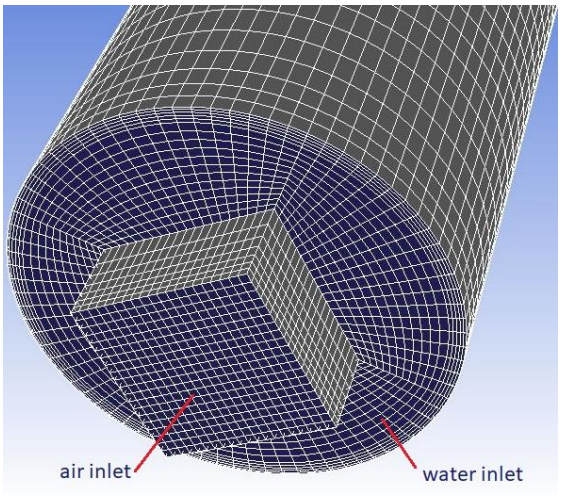

Figure 4-4: Velocity inlet boundary condition

Turbulence intensity and turbulence length scale are used for the **turbulence inlet boundary** conditions:

The turbulence intensity is defined as:

$$I = 0.16Re^{\left(\frac{-1}{8}\right)} \quad 4\text{-}3$$

And the turbulence length scale:

$$l = \frac{0.07D}{C_\mu^{\left(\frac{3}{4}\right)}} \quad 4\text{-}4$$

Where $C_\mu = 0.09$.

The Reynolds number in equation 4-3 is based on the hydraulic diameter of the inlet section.

The boundary condition at the **outlet** is set to pressure outlet with zero, gauge pressure.

The boundary condition for all the walls is non-slip condition. The surface roughness of the **walls** is also assumed zero (smooth wall), since this is quite close to zero for the transparent pipe used.

4.6 CFD approach

This section specifies the suggested CFD model for the task defined in this study.

4.6.1 The CFD model

It can be seen from the literature review in Chapter 2 that there is no general agreement regarding the CFD approach for two-phase gas-liquid flows. A general trend may be that VOF models were used more in earlier works and this has been moved to use of Eulerian-Eulerian model. VOF limitation in using one momentum equation does not capture the slip velocity between the phases and can only be used for very small slip velocities.

The mixture model may be used when the secondary phase is a dilute dispersed phase. A drift flux model for the slip velocity is used in this case. The flow pattern in this case is not considerable as there is a uniform distribution of phases in the flow domain. The mixture model cannot be used when phases are partly separated as in slug flow, churn and annular flow.

The multi fluid VOF model also called Eulerian-Eulerian VOF hybrid model, solves separate momentum equations for each phase. Hence, the velocity field will be captured precisely. Simultaneously, the VOF model, as a surface tracking model, captures the phase distribution and flow pattern can be perceived. The trend in using this model can be seen in recent publications from the literature review in Chapter 2.

While Multifluid Eulerian VOF model could be used for many applications of the multiphase flows, it is not perfect and there are still many details, which requires using this model with caution and not accepting the results obtained from it confidently. The problem is that the model still lacks two things: constitutive models which can model interphase effects and models which can take the effects of bubbles/droplets. These two models are also not independent of each other.

Phenomena as bubble coalescence and breakup, bubble entrainment in Taylor bubbles and other such phenomena involved, cannot be modelled by the multifluid Eulerian model. The same applies to droplets as well. Droplet entrainment in the wall film and also detachment from the wall film, may be important in annular flow regime. Hence, population balance equation has been used to deal with these effects. The equation has mainly been used for the bubbly flow and in some cases it has been used for droplets in annular flow regime. Coupling population balance equation with flow equation has a very high computational expense. This is not even straightforward in commercial CFD software and using it for engineering applications may not be an efficient option.

4.6.2 The choice of primary and secondary phases

Generally, the choice of primary and secondary phases is based on which phase is continuous and which phase is dispersed. Following this, for the gas-liquid flow the choice of primary phase and the secondary phase would rely on the flow pattern. In this manner, in bubble and slug flow, and partly churn flow, liquid is the primary phase and gas is the secondary phase and for higher gas flow rates, corresponding to churn turbulent and annular, the water is the secondary phase. If gas is supposed as the dispersed phase, the bubble dynamic is important and in the case of liquid as the secondary phase the droplet interaction with phases is more important. This approach is not favorable for the aim of this study, which is a unified CFD method for all flow patterns. The CFD model suggested in this study use air as the secondary phase. The choice is made based on the fact that the bubble dynamics have a major effect on

the flow pattern structure. Besides, the models used for the interfacial area concentration source terms are all developed for bubbles.

4.6.3 The operating conditions

The operating conditions are presented in Table 4-2:

Table 4-2: Operating conditions

Operating Pressure (Pa)	101325
Operating Density ($\frac{kg}{m^3}$)	1.225

The operational density is important since unlike the density-based solver, the pressure-based solver uses operating density as reference.

4.6.4 Solving details

The under-relaxation factors (URF) are used to stabilize the convergence behavior of discretized equations by introducing them in each iteration. In this way, they affect the convergence speed of the equations. Higher values of URFs may cause faster convergence but make the solution unstable and increase the risk of divergence. The default values of the URFs were reduced to avoid divergence for the transient solver. The value of URFs used are presented in Table 4-3:

Table 4-3: Under-relaxation values

Pressure	0.3
Momentum	0.3
Density	1
Body Forces	0.5
Volume Fraction	0.5
Turbulent Kinetic Energy	0.6
Turbulent Viscosity	0.5
Interfacial Area Concentration	0.1

The following discretization schemes have been used for the spatial discretization are as presented in Table 4-4:

Table 4-4: Discretization schemes

Gradient	Least Squares Cell Based
Momentum	Second Order Upwind
Volume Fraction	Second Order Upwind
Turbulent Kinetic Energy	Second Order Upwind
Turbulent Dissipation Rate	Second Order Upwind
Interfacial Area Concentration	Second Order Upwind

The time discretization scheme used is first order implicit.
Maximum number of iterations for each time step of transient calculation was set to 50 iterations. The time step size is chosen based on the maximum Courant number near the VOF interface. The Courant–Friedrichs–Lewy (CFL) number relates velocity of flow, cell size and the time step size. The CFL number for automatic time step adjustment was set to the value of

2. The maximum value for the residuals of all parameters was set to 0.001 as the convergence criteria.

The primary trials for solving the task was performed by starting a transient solution from the time zero. The whole volume was patched with one of the phases at time zero. It was found that the required time for the flow to be fully developed was up to seven seconds. This time corresponded to numerous hours of unnecessary simulation. To avoid this, a pseudo transient simulation was initiated first and the flow parameters were monitored to identify when the flow is fully developed. The convergence of the volume averaged void fraction value in the whole flow domain was monitored. The static pressure values were monitored for elevations of 1m, 2m and 3m. The void fraction convergence for these elevations was also monitored. The values were starting to oscillate about the mean values after an average of about 1500 iterations. The convergence never occurred at this situation due to the transient nature of the flow. After this, the solver was changed to transient and the flow was simulated for about two seconds for each case.
For the steady-state part of solution a coupled scheme was used, while for the transient part, phase coupled SIMPLE scheme used.
The turbulence model used is the RNG *k*-ε model. Both SST *k*-ω and RNG *k*-ε models are used in different publications for the type of the task as discussed in Chapter 2. Parsi et al. [10] compared these two models for gas liquid vertical churn flow. The results for both cases were relatively the same. In the primary simulations, this study found that the RNG *k*-ε turbulence model was more stable regarding convergence. Scalable wall functions has been used. The SST *k*-ω model is also insensitive to the grid close to the wall. A separate set of turbulence transfer equations for *k* and ε where used. This provides a more precise modeling of the turbulence.

4.6.5 Phase interactions

The use of constitutive models for phase interactions could have a significant effect both on convergence and the final simulation results. The drag force is generally the most important interphase interaction. The drag force in ANSYS Fluent is based on the interfacial area and the interfacial area as explained in section 3.3. ANSYS Fluent anisotropic drag coefficient model found to give a better convergence stability and accuracy of the results.

The non-drag interaction forces are known to have a minor effect in the accuracy of the results. The wall lubrication force as described in section 3.6, has been used. The Tomiyama model [16] has been used for the wall lubrication coefficient, C_{wl} in equation 3-28. For the lift force coefficient, C_l, in Equation 3-27, also the Tomiyama model [16] has been used. The virtual mass force is modeled as described by Equation 3-29. The virtual mass coefficient, C_{vm}, was set to 0.5.

5 Results, Discussions and Conclusions

The Task and the suggested CFD method for solving the problem was introduced in the previous chapter. The experimental reference for verifying the results was also introduced. Based on this, this chapter shows the results and compares them with the experiment. Further, the results have been analyzed and some deviation, which exists in the results, have been justified. Furthermore, the generalization of the suggested CFD method for two-phase gas-liquid flows has been discussed. Finally, the conclusions of this study and the way forward has been presented.

5.1 Simulation cases

Section 4.2 presented the experimental setup and the details regarding measuring liquid holdup and pressure gradient. A range of experiments were available from [25] for the 97mm pipe. A range of experiments which covered a broader flow pattern variation have been chosen. Table 5-1 shows the seven simulation cases used in this study:

Table 5-1: Simulation cases

Case number	Liquid superficial velocity (*m/s*)	Gas superficial velocity (*m/s*)
1		0.46
2		1.22
3		2.56
4	0.75	3.58
5		6.65
6		9.21
7		17.35

5.2 Flow pattern results

Although flow pattern maps are not accurate, they help us estimating the flow regime. Hence, flow pattern maps are used here as a guideline to follow the changes of flow pattern for the seven cases defined in section 5.1. FLOPATN [21] was introduced in section 2.4, is available as macros in an Excel program by Shoham [27]. According to the FLOPATN two-phase flow map, the location of the seven simulation cases are as shown in Figure 5-1:

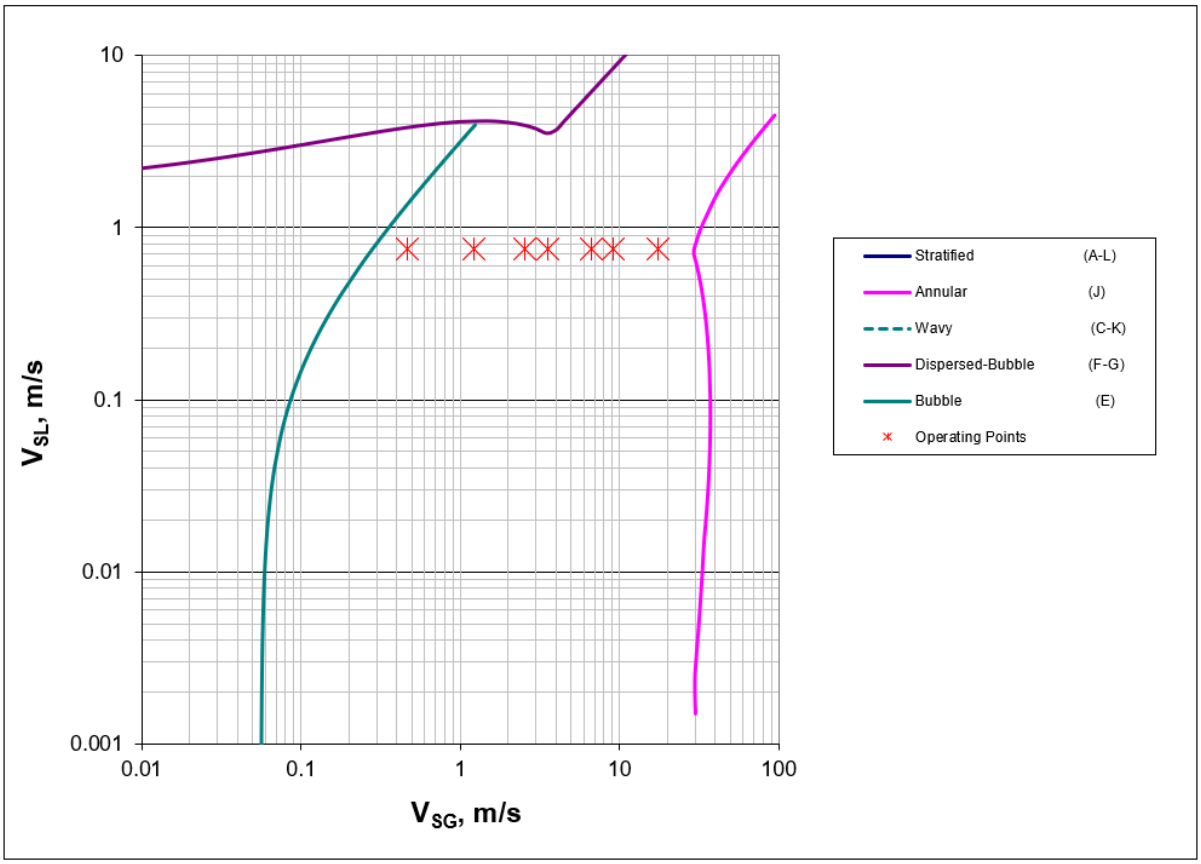

Figure 5-1: Flow pattern map derived by FLOPATN for the seven cases investigated

FLOPATN does not provide slug to churn boundary transition. It should be noted that the sharp boundaries presented in the flow map are not certain. As it has been emphasized by Pereyra et al. [21] these sharp transition boundaries should be considered as a transition band.

Based on their experiments, Capovilla et al. [25] introduced the following flow map, using Mishima & Ishii [23] bubble to slug/cap-bubble and slug/cap-bubble to churn transition boundaries. They used Schlegel et al. [24] for transition from churn to annular. Figure 5-2 shows the seven case points of this study in the flow pattern map introduced by Capovilla et al. [25].

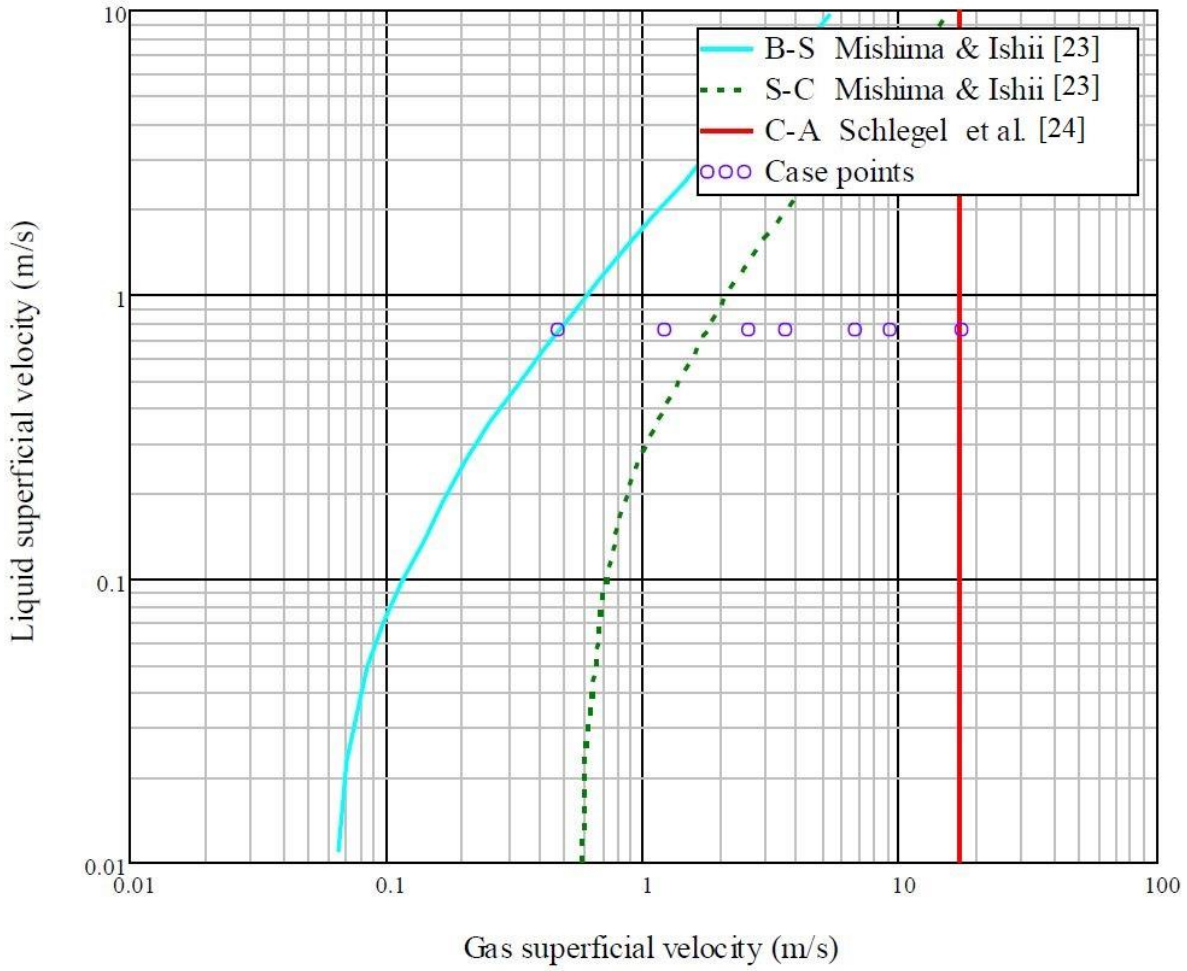

Figure 5-2: Flow pattern map based on [25], for the seven cases investigated. (B stands for Bubble, S for Slug, C for Churn and A for Annular)

The two flow pattern maps shown in Figure 5-1 and Figure 5-2 are not exactly similar due to uncertainty of transition boundaries. Capovilla et al. [25] observation are closer to the flow map introduced by them. The flow pattern observed from the CFD simulation results confirm this as well.

Table 5-2 shows the void fraction contour obtained by the CFD simulations, for the cross section of the pipe between the elevations 2m and 3m (Figure 4-2). The actual flow has a three-dimensional behavior and it is difficult to present it by an image. However, the void fraction contour presented in Table 5-2 and Table 5-3, can give an insight into the CFD simulation results.

Table 5-2: Void fraction contour for the lateral cross section of the pipe

Case	1	2	3	4	5	6	7
v_{sl}	0.75						
v_{sg}	0.46	1.22	2.56	3.58	6.65	9.22	17.34
Void Fraction 1 0.9 0.8 0.7 0.6 0.5 0.4 0.3 0.2 0.1 0	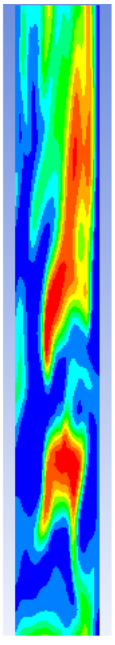	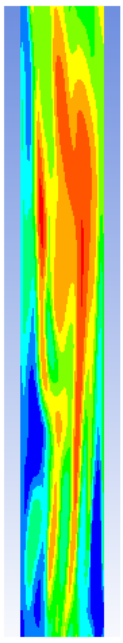	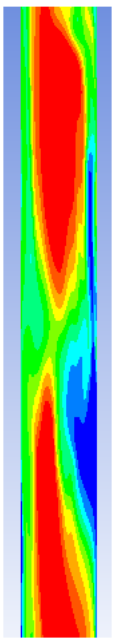	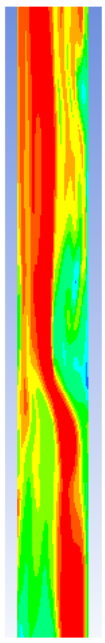	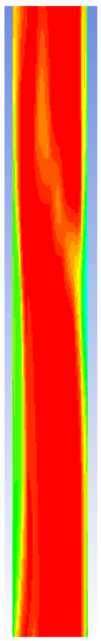	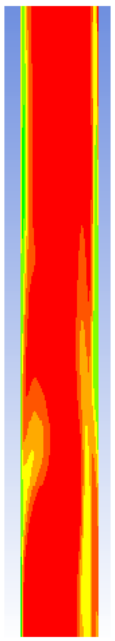	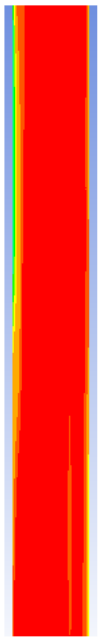
Observed Flow Pattern	Bubble/ Cap-bubble	Slug/cap-bubble	Churn	Churn	Churn	Churn	Churn/ Annular

Table 5-3 shows the contour of void fractions for the cross section of the pipe at the elevation of 2.5m (Figure 4-2).

Table 5-3: Contour of void fraction for the cross section of the pipe

Void Fraction				Observed Flow Pattern
Case	v_{sl}	v_{sg}		
1	0.75	0.46	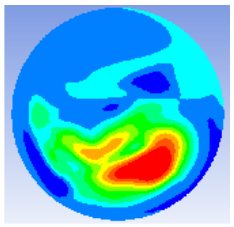	Bubble/ Cap-bubble
2		1.22	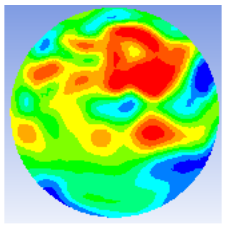	Slug/cap-bubble
3		2.56	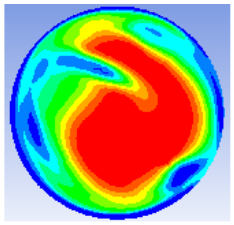	Churn
4		3.58	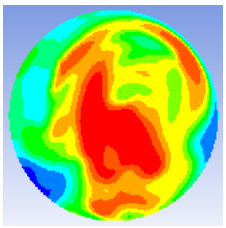	Churn
5		6.65	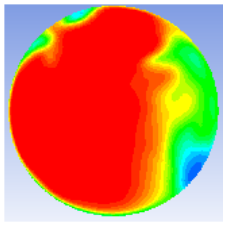	Churn
6		9.22	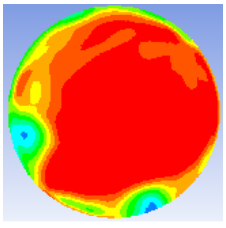	Churn

7		17.34	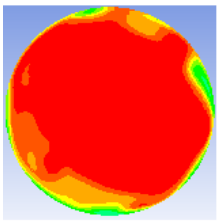	Churn/ Annular

The void fraction for Case 1 shows dispersed bubbles (colors between blue and red) and some larger bubbles (red color). It should be noted that the exact shape of bubbles cannot be observed from these contours. The VOF model uses a linear interface reconstruction and an extremely fine mesh is required to be able to visualize a more realistic bubble shape.

The coalescence of bubbles into longer and wider uniform bubbles could be observed from the contours of void fraction for Case 2. Case 3 shows both behaviors of slug and churn flows with long and wide bubbles and interfacial waves. The cases 4 to 6 are all having churn flow characteristics. There is a distinct boundary between the gas and liquid phases. The waves at the interface of gas and liquid are suppressed as the gas superficial velocity increases.

Case 7 shows both behaviors of churn and annular flows, with the liquid film and the gas core and simultaneously very small waves at the interface. In general, the flow patterns obtained from the CFD simulations agree with the observations of Capovilla et al. [25].

Many of the aspects of the three-dimensional flows cannot be presented by these images. In order to show this, an image of the three-dimensional domain for two of the cases are represented here. Figure 5-3 shows velocity vectors for a section of the case 4 pipe, colored by the phase fraction. The flow has a completely three-dimensional structure and the gas moves in a swirling pattern through the pipe, creating recirculation zones and falling liquid film, which can be observed on the right side of the Figure 5-3.

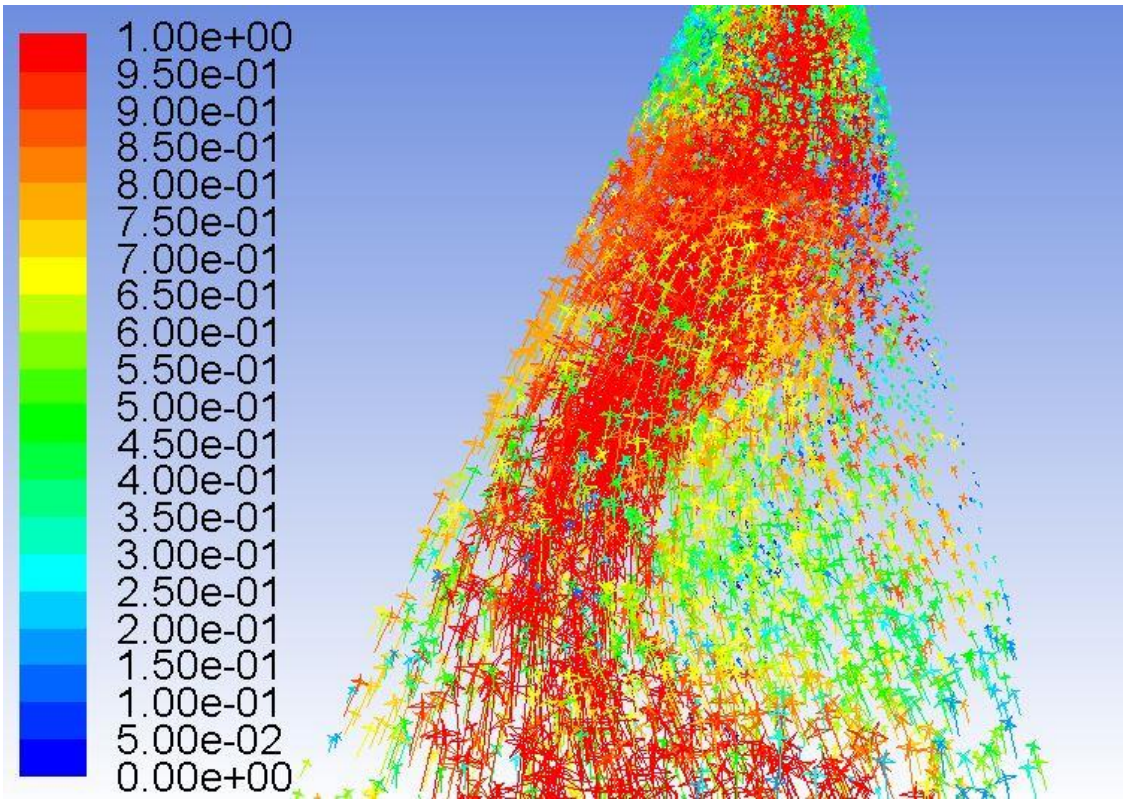

Figure 5-3: Velocity vectors colored by void fraction for case 4

Figure 5-4 shows the velocity vectors for a part of the case 1 pipe. The velocity vectors are colored by the phase fraction. The bubbles are coalescing and form a larger bubble which speeds up the liquid around it. A swirling area is formed in the wake of the bubble.

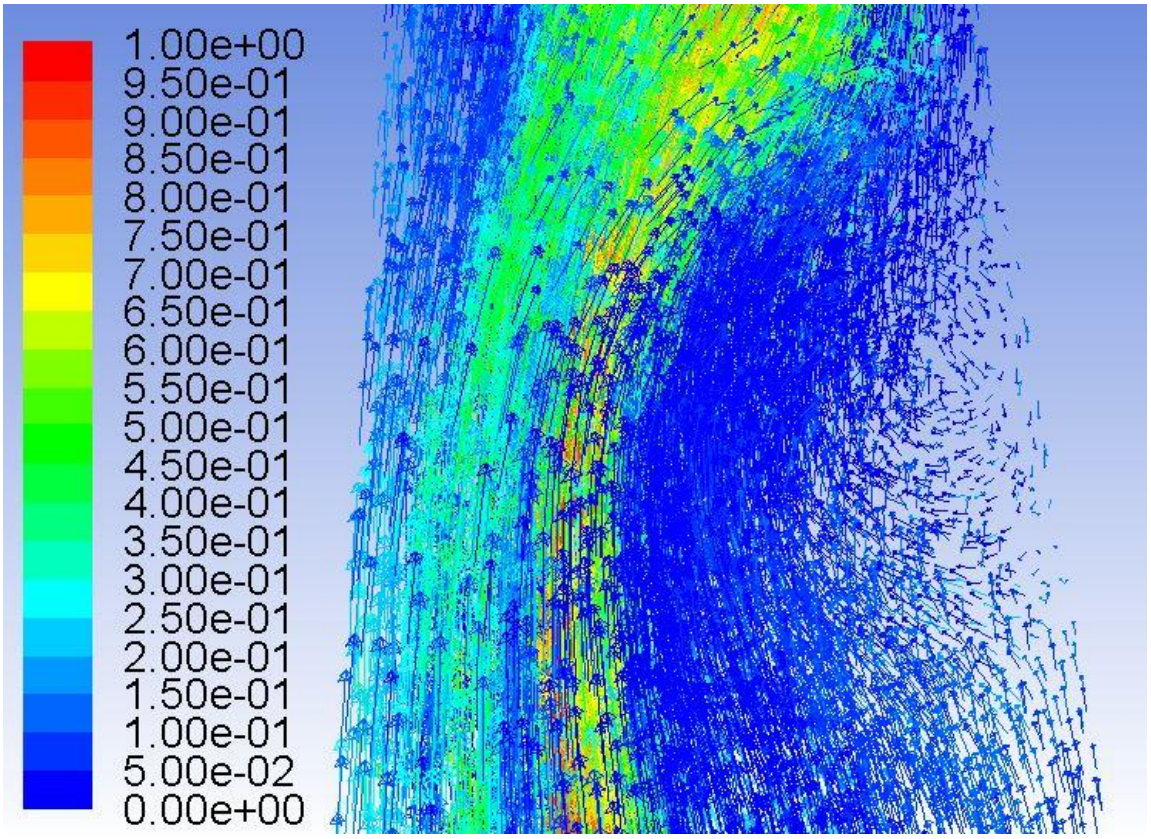

Figure 5-4: Velocity vectors colored by void fraction for case 1

5.3 Beggs & Brill correlation

Empirical and semi-empirical correlations used for multiphase gas-liquid flows, has been discussed in Chapter 2. No correlation can give a precise prediction of flow pattern, void fraction and pressure gradient for gas liquid flows. However, they give a very convenient basis for estimation of these properties. Beggs & Brill correlation for inclined pipes [43] has been used extensively in the oil and gas industry. Although it is not the focus of this work, it has been decided to represent Beggs & Brill correlation results for the case study here as an additional information. The Beggs & Brill model programmed with the Mathcad software and corresponding calculations are presented in Appendix A.

5.4 Void fraction results

Most of the publications have reported void fraction/liquid holdup results for certain elevations where the sensors were installed. Figure 2-2 shows an example of such transient void fraction measurement. Capovilla et al. [25] reported the liquid holdup $(1-\alpha)$ for the whole pipe by a sudden closure of the air and water flows and then measuring the water volume using a sensor at the bottom of the pipe. This average void fraction value is easier to use since its value is relatively constant for the whole volume and the specified superficial liquid and gas velocities. It is worth mentioning that similar results have been observed from the CFD simulations; where the instantaneous void fraction measurements for a specific elevation fluctuate considerably over time, while the average void fraction for the whole domain is relatively constant over time. However, this method may not be quite precise, because of the transient phase when the valves are closed.

Figure 5-5 shows the void fraction results for the whole vertical pipe, obtained from the CFD simulations. The CFD results, experimental results and the value obtained from the Beggs & Brill correlation are presented in the graph for the seven cases of this study.

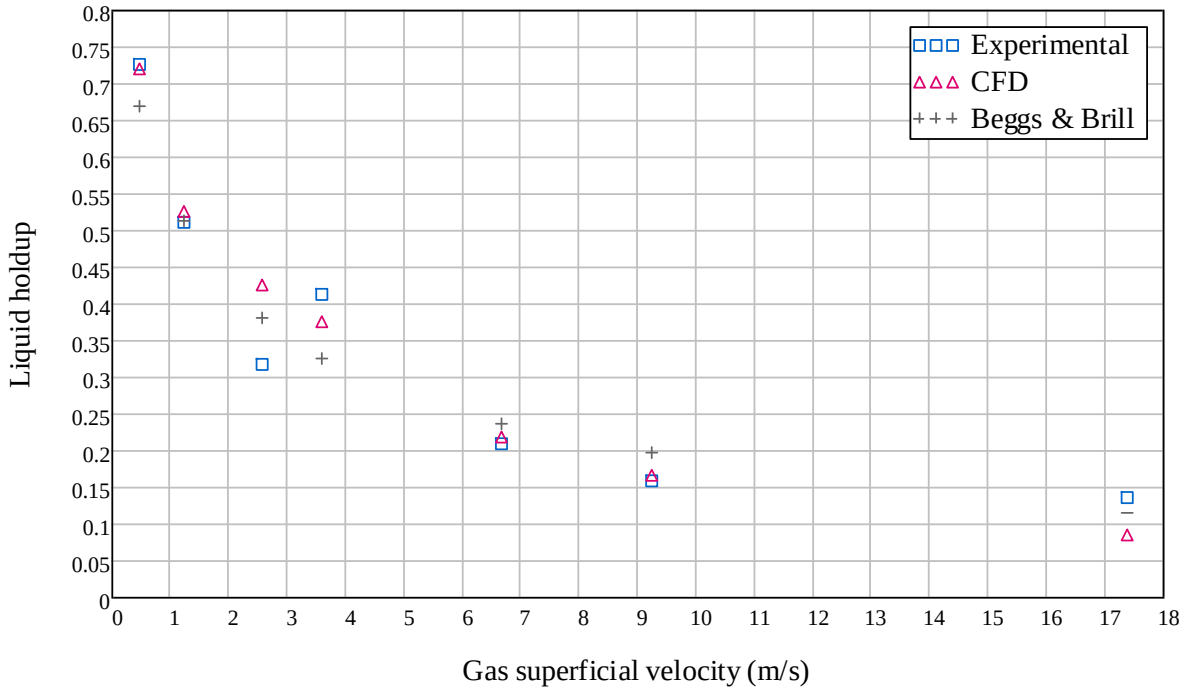

Figure 5-5: Liquid holdup results for the seven cases investigated

Case 1 and 2, which are in the bubble/cap-bubble flow regime area show a very good agreement with the experimental data set. The bubble coalescence and break-up models used are Hibiki & Ishii [37], as described in section 3.9. These models are known to have a good performance for the bubbly flow.

Case 3 and 4 have larger deviation comparing to the other cases. There is a jump in the experimental results for liquid holdup for these cases, which cannot be justified. This could be due to measurement errors, since the same pattern could not be seen in experiments performed by Capovilla et al. [25] with other pipes. Further experiments are needed to identify if the source of error is the difficulty with the measurement method used for the experiments or it is due to incapability of the CFD model to capture interfacial waves.

Case 5 and 6 also show a very good agreement with the experimental data set. These cases are in the churn flow regime. The effect of interfacial waves is less due to higher damping of these waves in the high velocity gas core.

For case 7, which is in the churn-annular transition boundary, the deviation of the results is also high. This could be as a result of the CFD model incapability in capturing droplet dynamics. However, further investigation is required in the annular flow area to analyze this issue. Zahedi et al. [13] also reported this issue with the droplet dynamics.

It is also interesting to see that Beggs & Brill correlation performance is relatively good. Some other publications have also shown Beggs & Brill results; for example, Hernandez-Perez [44] showed a relatively good agreement for a 67mm pipe.

5.5 Pressure gradient results

The pressure gradient is the sum of frictional and gravitational pressure drop, where the latter one has a dominant effect. In fact, the frictional pressure drop gradient comparing to

gravitational is so small that it could be neglected. This has a negative effect for our study, since the errors in the liquid holdup calculations are summed up in pressure gradient calculations as well.

Figure 5-6 compares the CFD results and experimental results for the seven cases investigated. The time averaged value of the pressure gradient is reported for the CFD simulation results. This value fluctuates constantly over time for the cross sections it has been measured. Hence, time averaged values are presented. The predicted pressure gradient from Beggs & Brill is also presented.

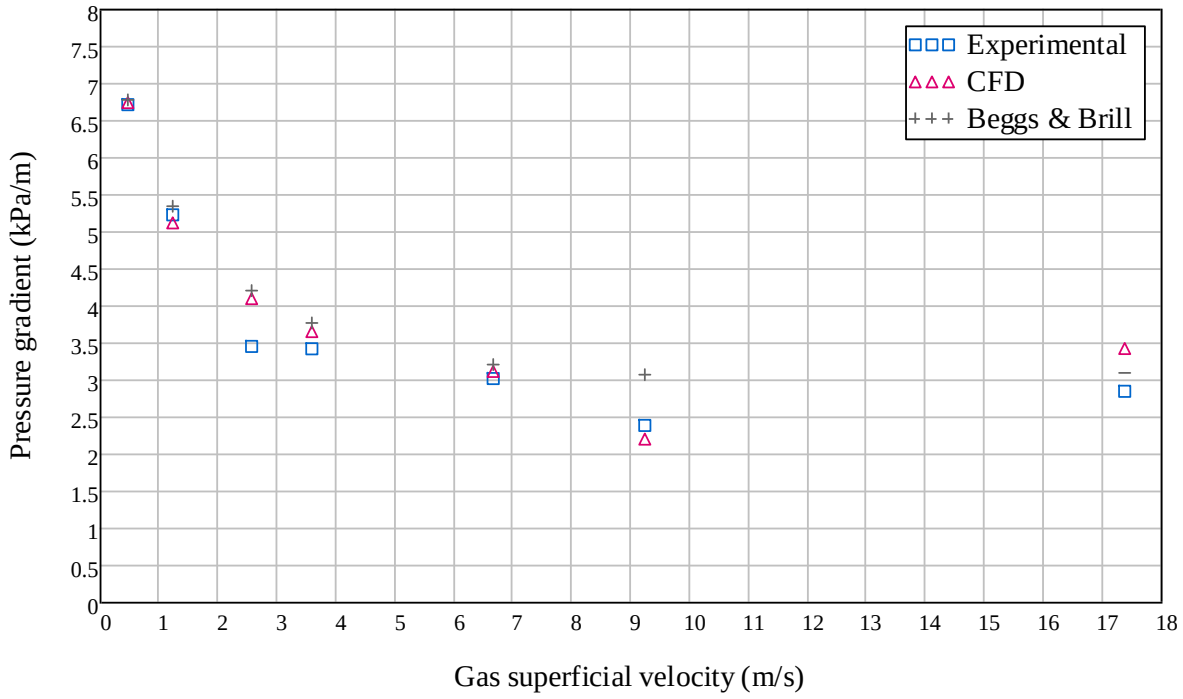

Figure 5-6: Pressure gradient results

Case 1 and 2, which are in the bubble/cap-bubble flow regime area, show a very good agreement with the experimental dataset, while case 3 and 4 show a higher deviation. This is the same for the void fraction (liquid holdup) results and as mentioned, since the gravitational pressure has a dominant effect, the errors in the void fraction affect pressure gradient results.

Case 7 also shows a higher deviation comparing to the cases 5 and 6. As mentioned in section 5.4, this could be due to incapability of the CFD model used in capturing droplet dynamics and further investigation in the annular flow regime area is required to confirm this.

The pressure gradients obtained from the Beggs & Brill correlation are also in a relatively good agreement for most of the cases studied here.

6 Conclusions

The CFD methods which had been used previously for a vertical upward gas-liquid flow and the available CFD approaches to deal with this problem studied. Different CFD approaches and closure models were investigated and based on this, a CFD method which could handle variety of flow regimes was adopted. In order to verify the capability of this suggested CFD method, an experimental dataset selected. This experimental dataset had investigated two-phase upward vertical air-water flow for three different pipe diameters. The dataset for the 97mm pipe was used for verification of CFD results, since it covered a broader range of flow patterns. The experimental dataset had investigated liquid holdup for the whole pipe and the pressure gradient.

A task was defined for a range of cases covering from bubble/cap bubble flow pattern to churn/annular flow pattern based on the experimental dataset. The main results obtained from the study and investigation of CFD models used for solving the defined task are summarized in the following.

1. The multifluid Eulerian VOF model, where separate conservation equations are used for each phase, can predict a specific flow pattern, but the constraint of using constant bubble or droplet diameter limits the application for a broader range of flow patterns. A single CFD model is incapable of predicting different flow patterns. The bubble or droplet size also should be driven from available correlations or previous experiments. This is also challenging when there are various bubble or droplet sizes and shapes. For example, in bubble/cap-bubble flow pattern.
2. The three-fluid CFD model suggested can predict different flow patterns, using a single CFD model. The separate Eulerian conservation equations for each phase gives a precise prediction of the velocity field and the VOF model works as the interfaces tracking model. The interfacial area concentration equation captures the bubble dynamics and provides a better prediction of the flow patterns. The use of IAC equation relaxes the constraint of using constant bubble/droplet diameter and a better prediction of flow pattern can be achieved.
3. Comparing the obtained CFD results with the experimental results shows that the suggested model has a very good performance for bubble and cap-bubble flow regimes. This could be related to the efficiency of the coalescence/breakup models used. For the transition area between cap bubble and churn flow patterns the model had a worse performance comparing to other cases.
4. The dominant phenomena in churn-annular and annular flow is the interaction between the liquid droplets in the gas core and the wall film; unlike the bubble, cap-bubble, slug and slug-churn regime where the bubble dynamic is dominant. Hence, extra equations may be needed to capture droplet entrainment to wall film and detachment from it.
5. A one group IAC model has limitations since the coalescence/breakup model cannot deal with different bubble/droplet diameters and shapes, spherical/cap, at the same time. A two group or a multi-group IAC model may be required for better results. However, it requires more computational effort and can increase computation time significantly.

6. A review of flow pattern maps and prediction model shows that the uncertainty exists by comparing different models. The majority of the research has been done on small diameter pipes, which are smaller than the value defined by equation 1-1, and the results cannot be generalized for larger pipes. The constants used for constitutive models are based on data fitting for small diameter pipes and may not be appropriate for larger diameter pipes. However, flow pattern maps may be used as a guideline for a rough estimate of possible flow patterns.

6.1 Future work

A major part of the time for this study was used for trying and checking the efficiency of different CFD models and constitutive equations for the task defined. The literature available for CFD modeling of vertical gas-liquid flows is relatively young and there are many areas, which require further research. A multifluid VOF model used with interfacial area concentration seems to be a promising method in dealing with gas-liquid flows. However, more research is required in this area. CFD simulations are time consuming and this makes the work more difficult.

The use of two-group or a multi-group interfacial area concentration equation should be investigated. More comprehensive models for bubble coalescence and breakup, are also required for better modeling of gas-liquid flows. There are some publications, which have researched modeling of annular flows and droplet dynamics. Yet, there is a large gap, and more research is needed for implementation of these models in the CFD models.

References

[1] I. Kataoka og M. Ishii, «Drift flux model for large diameter pipe and new correlation for pool void fraction,» *International Journal of Heat and Mass Transfer,* vol. 30, nr. 9, pp. 1927-1939, 1987.

[2] M. Behnia, «Most accurate two-phase pressure-drop correlation identified,» *Oil and Gas Journal,* vol. 89, nr. 37, 1991.

[3] M. A. Woldesemayat og A. J. Ghajar, «Comparison of void fraction correlations for different flow patterns in horizontal and upward inclined pipes,» *International Journal of Multiphase Flow,* vol. 33, nr. 4, pp. 347-370, 2007.

[4] K. H. Bendiksen, D. Malnes, R. Moe og S. Nuland, «The Dynamic Two-Fluid Model OLGA: Theory and Application,» *SPE Production Engineering,* 1991.

[5] R. Belt, B. Djoric, S. Kalali, E. Duret og D. Larrey, «Comparison of commercial multiphase flow simulators with experimental and field databases,» Cannes, 2011.

[6] C. L. Pauchon og H. Dhulesia, «TACITE: A Transient Tool for Multiphase Pipeline and Well Simulation,» 1994.

[7] Y. Liu, W. .. Z. Li og S. L. Quan, «A self-standing two-fluid CFD model for vertical upward two-phase annular flow,» *Nuclear Engineering and Design,* nr. 241, p. 1636–1642, 2011.

[8] D. Dakshinammorthy, Y. Dai og M. Agrawal, «CFD Modeling of Bubbly, Slug and Annular Flow Regimes in Vertical Pipelines,» Texas, 2013.

[9] M. Abdulkadir, V. Hernandez-Perez, S. Lo, I. Lowndes og B. Azzopardi, «Comparison of experimental and Computational Fluid Dynamics (CFD) studies of slug flow in a vertical riser,» *Experimental Thermal and Fluid Science,* vol. 63, pp. 468-483, 2015.

[10] M. Parsi, M. Agrawal, V. Srinivasan, R. E. Vieira, C. F. Torres, B. S. McLaury, S. A. Shirazid, E. Schleicher og U. Hampel, «Assessment of a hybrid CFD model for simulationof complex vertical upward gas-liquid churn flow,» *Chemical Engineering Research and Design,* pp. 71-84, 2016.

[11] C. Peña-Monferrer, A. Passalacqua, S. Chiva og J. L. Muñoz-Cobo, «CFD modelling and validation of upward bubbly flow in an adiabaticvertical pipe using the quadrature method of moments,» *Nuclear Engineering and Design,* nr. 301, pp. 320-332, 2016.

[12] F. Tocci, F. Bos og R. Henkes, «CFD for multiphase flow in vertical risers,» Cannes, 2017.

[13] P. Zahedi, J. Zhang, H. Arabnejad, B. S. McLaury og S. A. Shirazi, «CFD simulation of multiphase flows and erosion predictions under annular flow and low liquid loading conditions,» *Wear,* Vol. %1 av %2376-377, pp. 1260-1270, 2017.

[14] S. Abood, M. Abdulwahid og M. Almudhaffar, «Comparison between the experimental and numerical study of (air-oil) flow patterns in vertical pipe,» *Case Studies in Thermal Engineering,* 2019.

[15] E. Adaze, H. Badr og A. Al-Sarkhi, «CFD modeling of two-phase annular flow toward the onset of liquid film reversal in a vertical pipe,» *Journal of Petroleum Science and Engineering,* nr. 175, pp. 755-774, 2019.

[16] A. Tomiyama, «Struggle with computational bubble dynamics,» Lyon, France, 1998.

[17] T. Hibiki og M. Ishii, «One-group interfacial area transport of bubbly flows in vertical round tubes,» *International Journal of Heat and Mass Transfer,* vol. 43, nr. 15, pp. 2711-2726, 2000.

[18] Q. Wu, S. Kim, M. Ishii og S. G. Beus, «One-group interfacial area transport in vertical bubbly flow,» *International Journal of Heat and Mass Transfer,* vol. 41, nr. 8-9, pp. 1103-1112, 1998.

[19] B. Wu, M. Firouzi, T. Mitchell, T. E. Rufford og C. Leonardi, «A critical review of flow maps for gas-liquid flows in vertical pipes and annuli,» *Chemical Engineering Journal,* vol. 326, pp. 350-377, 2017.

[20] O. Bratland, Pipe Flow 2: Multi-phase Flow Assurance, drbratland.com, 2013.

[21] E. Pereyra, C. Torres, R. Mohan, L. Gomez, G. Kouba og O. Shoham, «A methodology and database to quantify the confidence level of methods for gas–liquid two-phase flow pattern prediction,» *Chemical Engineering Research and Design,* vol. 90, nr. 4, pp. 507-513, 2012.

[22] Y. Taitel, D. Bornea og A. E. Dukler, «Modelling flow pattern transitions for steady upward gas-liquid flow in vertical tubes,» *AIChE J.* , vol. 26, p. 345–354, 1980.

[23] K. Mishima og M. Ishii, «Flow regime transition criteria for upward two-phase flow in vertical tubes,» *International Journal of Heat and Mass Transfer,* vol. 27, nr. 5, pp. 723-737, 1984.

[24] J. P. Schlegel, P. Sawant, S. Paranjape, B. Ozar, T. Hibiki og M.Ishii, «Void fraction and flow regime in adiabatic upward two-phase flow in large diameter vertical pipes,» *Nuclear Engineering and Design,* vol. 239, nr. 12, pp. 2864-2874, 2009.

[25] M. S. Capovilla, R. P. Coutinho, P. C. d. Sousa og P. J. Waltrich, «Experimental investigation of upward vertical two-phase high-velocity flows in large-diameter pipes,» *Experimental Thermal and Fluid Science,* vol. 102, pp. 493-505, 2019.

[26] D. Barnea, «A unified model for predicting flow-pattern transitions for the whole range of pipe inclinations,» *Int. J. Multiphase Flow,* vol. 13, nr. 1, pp. 1-12, 1987.

[27] O. Shoham, Mechanistic modeling of gas-liquid two-phase flow in pipes, Society of Petroleum Engineers, 2006.

[28] N. K. Omebere-Iyari og B. J. Azzopardi, «A Study of Flow Patterns for Gas/Liquid Flow in Small Diameter Tubes,» *Chemical Engineering Research and Design,* vol. 85, nr. 2, pp. 180-192, 2007.

[29] ANSYS-Fluent, «ANSYS Fluent 17.2 user's guide,» 2016.

[30] M. Manninen, V. Taivassalo og S. Kallio, «On the mixture model for multiphase flow,» VTT Energy, Espoo, 1996.

[31] M. Ishii og K. Mishima, «Two-fluid model and hydrodynamic constitutive relations,» *Nuclear Engineering and Design,* vol. 82, nr. 2-3, pp. 107-126, 1984.

[32] G. H. Yeoh og J. Tu, Computational Techniques for Multiphase Flows, 1 red., Elsevier, 2009.

[33] A. A. Troshko og Y. A. Hassan, «Law of the wall for two-phase turbulent boundary layers,» *International Journal of Heat and Mass Transfer,* vol. 44, nr. 4, pp. 871-875, 2001.

[34] M. Ishii og T. Hibiki, Thermo-Fluid dynamics of two-phase flow, 1 red., New York,: Springer Science+Business Media, Inc, 2006.

[35] M. L. d. Bertodano, «Turbulent Bubbly Flow in a Triangular Duct,» Rensselaer Polytechnic Institute, New York, 1991.

[36] T. Chuang og T. Hibiki, «Vertical upward two-phase flow CFD using interfacial area transport equation,» *Progress in Nuclear Energy,* vol. 85, pp. 415-427, 2015.

[37] T. Hibiki og M. Ishii, «One-group Interfacial Area Transport of Bubbly Flows in Vertical Round Tubes,» *International Journal of Heat and Mass Transfer,* vol. 43, p. 2711–2726, 2000.

[38] M. Ishii og S. Kim, «Micro Four-Sensor Probe Measurement of Interfacial Area Transport for Bubbly Flow in Round Pipes,» *Nuclear Engineering and Design,* vol. 205, p. 123–131, 2001.

[39] W. Yao og C. Morel, «Volumetric Interfacial Area Prediction in Upward Bubbly Two-Phase Flow,» *International Journal of Heat and Mass Transfer,* vol. 47, pp. 307-328, 2004.

[40] J. P. Schlegel, T. Hibiki, X. Shen, S. Appathurai og H. Subramani, «Prediction of interfacial area transport in a coupled two-fluid model computation,» *Journal of Nuclear Science and Technology,* vol. 54, nr. 1, pp. 58-73, 2017.

[41] M. S. Capovilla, R. P. Coutinho, P. C. d. Sousa og P. J. Waltricha, «Experimental investigation of upward vertical two-phase high-velocity flows in large-diameter pipes,» *Experimental Thermal and Fluid Science,* vol. 102, pp. 493-505, 2019.

[42] V. Hernandez-Perez, M. Abdulkadir og B. J. Azzopardi, «Grid Generation Issues in the CFD Modelling of Two-Phase Flow in a Pipe,» *The Journal of Computational Multiphase Flows,* vol. 3, nr. 1, pp. 13-26, 2011.

[43] D. H. Beggs og J. P. Brill, «A Study of Two-Phase Flow in Inclined Pipes,» *Journal of Petroleum Technology*, vol. 25, nr. 5, 1973.

[44] V. Hernandez-Perez, *Gas-liquid two-phase flow in inlined pipes*, University of Nottingham, 2008.

Appendices

Appendix A

Beggs & Brill Method [43]

Input Variables

Inclination angle

$\theta := 90\,deg$

Pipe diameter

$D := 97\,mm$

Section length

$L := 1\,m$

liquid density

$\rho_l := 998.2\frac{kg}{m^3}$

Gas density

$\rho_g := 1.225\frac{kg}{m^3}$

Liquid density

$\mu_l := 0.001003\,Pa\cdot s$

Gas density

$\mu_g := 1.7894\,10^{-5}\,Pa\cdot s$

Surface tension

$\sigma := 0.072\frac{N}{m}$

Liquid superficial velocity

$v_{sl} := 0.75\frac{m}{s}$

gas superficial velocity

$v_{sg} := 1.223\frac{m}{s}$

Pipe wall roughness

$\varepsilon := 0mm$

Beggs & Brill Method

Inlet liquid content

$$\lambda_l := \frac{v_{sl}}{v_{sl} + v_{sg}} = 0.38$$

mixed velocity

$$v_m := v_{sl} + v_{sg} = 1.973\frac{m}{s}$$

Froud number

$$NFr := \frac{v_m^2}{g \cdot D} = 4.092$$

Transition boundaries

$$L1 := 316\lambda_l^{0.302}$$

$$L2 := 0.0009252\lambda_l^{-2.4684}$$

$$L3 := 0.10\lambda_l^{-1.4516}$$

$$L4 := 0.50\lambda_l^{-6.738}$$

FlowRegime :=
- (return "Segregated") if $\lambda_l < 0.01 \wedge NFr < L1 \vee \lambda_l \geq 0.01 \wedge NFr < L2$
- (return "Transition") if $\lambda_l \geq 0.01 \wedge L2 \leq NFr \leq L3$
- (return "Intermittent") if $0.01 \leq \lambda_l < 0.4 \wedge L3 < NFr \leq L1 \vee \lambda_l \geq 0.4 \wedge L3 < NFr \leq L4$
- (return "Distributed") if $\lambda_l < 0.4 \wedge NFr \geq L1 \vee \lambda_l \geq 0.4 \wedge NFr > L4$

a :=
- return 0.980 if FlowRegime = "Segregated"
- return 0.845 if FlowRegime = "Intermittent"
- return 1.065 if FlowRegime = "Distributed"
- return 0 otherwise

b :=
- return 0.4846 if FlowRegime = "Segregated"
- return 0.5351 if FlowRegime = "Intermittent"
- return 0.5824 if FlowRegime = "Distributed"
- return 0 otherwise

$$c := \begin{cases} \text{return } 0.0868 \text{ if FlowRegime} = \text{"Segregated"} \\ \text{return } 0.0173 \text{ if FlowRegime} = \text{"Intermittent"} \\ \text{return } 0.0609 \text{ if FlowRegime} = \text{"Distributed"} \\ \text{return } 0 \text{ otherwise} \end{cases}$$

$$NLv := v_{sl} \cdot \left(\frac{\rho_l}{g \cdot \sigma} \right)^{\frac{1}{4}} = 4.599$$

$$C := \begin{cases} \left[\text{return } \left(1 - \lambda_l\right) \cdot \ln\left(0.011 \lambda_l^{-3.768} \cdot NLv^{3.539} \cdot NFr^{-1.614}\right) \right] \text{ if FlowRegime} = \text{"Segregated"} \\ \left[\text{return } \left(1 - \lambda_l\right) \cdot \ln\left(2.960 \lambda_l^{0.3050} \cdot NLv^{-0.4473} \cdot NFr^{0.0978}\right) \right] \text{ if FlowRegime} = \text{"Intermittent"} \\ (\text{return } 0) \text{ if FlowRegime} = \text{"Distributed"} \\ \text{return } 0 \text{ otherwise} \end{cases}$$

$$\psi := \begin{cases} \left[\text{return } 1 + C \cdot \left[\sin(1.8\theta) - 0.333(\sin(1.8\theta))^3 \right] \right] \text{ if FlowRegime} = \text{"Segregated"} \vee \text{FlowRegime} = \text{"Intermittent"} \\ (\text{return } 1) \text{ otherwise} \end{cases}$$

$$HL0 := \frac{a \cdot \lambda_l^{\,b}}{NFr^{c}} = 0.491$$

$$HL := \begin{cases} \text{return } (\psi \cdot HL0) \text{ if FlowRegime} \neq \text{"Transition"} \\ \left[\text{return } \left(\frac{L3 - NFr}{L3 - L2} \right) \cdot \left(\frac{0.980 \lambda_l^{0.4846}}{NFr^{0.0868}} \right) + \left(1 - \frac{L3 - NFr}{L3 - L2} \right) \cdot \left(\frac{0.845 \lambda_l^{0.5351}}{NFr^{0.0173}} \right) \right] \text{ otherwise} \end{cases}$$

Inlet void fraction

$$x := \frac{v_{sg}}{v_{sg} + v_{sl}} = 0.62$$

Mixed viscosity

$$\mu_m := \left(\frac{x}{\mu_g} + \frac{1 - x}{\mu_l} \right)^{-1} = 2.856 \times 10^{-5} \frac{kg}{m \cdot s}$$

Mixed density

$$\rho_m := \left(\frac{x}{\rho_g} + \frac{1 - x}{\rho_l} \right)^{-1} = 1.975 \frac{kg}{m^3}$$

Mixed Reynolds

$$Re_m := \frac{\rho_m \cdot v_m \cdot D}{\mu_m} = 1.324 \times 10^{4}$$

Mixed friction coefficient

$$f_m := \left[\frac{1}{-1.8\cdot\log\left[\left(\frac{\varepsilon}{3.7\cdot D}\right)^{1.11} + \frac{6.9}{Re_m}\right]}\right]^2 = 0.029$$

$$y := \frac{\lambda_l}{HL^2} = 1.44$$

$$S := \begin{cases} \left[\text{return } \frac{\ln(y)}{\left(-0.0523 + 3.182\ln(y) - 0.8725\ln(y)^2 + 0.01853\ln(y)^4\right)}\right] & \text{if } y < 1 \vee y > 1.2 \\ (\text{return } \ln(2.2\cdot y - 1.2)) & \text{otherwise} \end{cases}$$

$$f_{tp} := f_m\cdot e^S = 0.041$$

$$\rho_s := HL\cdot\rho_l + (1 - HL)\cdot\rho_g = 513.512\frac{kg}{m^3}$$

Results

Frictional pressure loss

$$\Delta p_f := \frac{f_{tp}\cdot\rho_m\cdot v_m^2\cdot L}{2\cdot D} = 1.639\,Pa$$

Liquid holdup

$$HL = 0.514$$

Void fraction

$$\alpha := 1 - HL = 0.486$$

Gravitational pressure loss

$$\Delta p_s := \rho_s\cdot g\cdot L = 5.036\times 10^3\cdot Pa$$

Total pressure loss

$$\Delta p_{total} := \Delta p_f + \Delta p_s = 5.037\times 10^3\,Pa$$